ACR No. 4I25

NATIONAL ADVISORY COMMITTEE FOR AERONAUTICS

WARTIME REPORT

ORIGINALLY ISSUED

September 1944 as
Advance Confidential Report 4I25

AN INVESTIGATION OF 0.15-CHORD AILERONS ON A LOW-DRAG TAPERED WING AT HIGH SPEEDS

By Edmund V. Laitone

Ames Aeronautical Laboratory
Moffett Field, California

WASHINGTON

NACA ACR No. 4I25

NATIONAL ADVISORY COMMITTEE FOR AERONAUTICS

ADVANCE CONFIDENTIAL REPORT

AN INVESTIGATION OF 0.15-CHORD AILERONS ON A LOW-DRAG TAPERED WING AT HIGH SPEEDS

By Edmund V. Laitone

SUMMARY

Tests of 0.15-wing-chord, internally balanced ailerons on a low-drag tapered wing were made at Mach numbers up to 0.75. The corresponding Reynolds number range was from 5,000,000 to 13,800,000. Both a normal-profile and a beveled, trailing-edge aileron were tested without a seal and with a partial seal. In addition to the usual aileron characteristics, the pitching-moment increments due to the aileron deflections were measured in order that the effect of Mach number on the aileron reversal speed could be estimated.

No severe compressibility effects were encountered until a Mach number of 0.725 was exceeded. The rolling-moment coefficient was found to increase with Mach number at a rate much less than that given by $1/\sqrt{1-M^2}$. The data indicated a tendency toward overbalance of the hinge moment of balanced ailerons as the speed increased.

INTRODUCTION

The high maneuverability required of modern pursuit airplanes, together with their large size and high speed, makes close balancing of the aileron hinge moments imperative. It has been found that compressibility effects may radically change the aileron characteristics at high speeds. Frequently ailerons which are closely balanced from tests at low speeds become overbalanced at high speeds. At present there is no reliable procedure for making allowance for the effects of compressibility on the aileron characteristics other than increasing the rolling moment by the factor $1/\sqrt{1-M^2}$ in which M is Mach number. The tests described in this report were

made to investigate the behavior at high Mach numbers of representative internally balanced ailerons on a low-drag tapered wing.

APPARATUS AND METHODS

The model used for these tests was a semispan, low-drag (NACA 66-series profile) tapered wing (fig. 1) geometrically similar to the one used for the tests reported in reference 1. The model was mounted in the 16-foot wind tunnel of the Ames Aeronautical Laboratory, Moffett Field, Calif., with the root chord parallel to the tunnel wall (fig. 2). The wing spar and aileron shaft extended through the tunnel wall. A single support strut was attached at the 0.75-chord point adjacent to the inboard end of the aileron (figs. 2 and 3).

The wing surfaces were smooth except during the tests for which the description "roughness at 0.10c" is used. For this condition, a 3/8-inch-wide strip of No. 100 carborundum particles was applied at the 0.10-wing-chord line along the entire span of the upper and lower surfaces.

The aileron chord aft of the hinge line was 0.15 of the wing chord. The aileron span was 0.41 of the wing semispan, and the inboard end of the aileron was at the midpoint of the wing semispan (fig. 1). The normal-profile aileron had the same profile as the low-drag wing section and a nose-balance chord of 0.60 of the aileron chord (fig. 4). The beveled aileron had a thickened and beveled trailing-edge portion and a nose-balance chord of 0.42 of the aileron chord (fig. 5). The variation from the normal profile ended abruptly at the inboard end of the aileron but, at the outboard end, was faired into the wing tip.

Both ailerons were tested unsealed and partially sealed with normal cover plates (figs. 4 and 5). In addition, the partially sealed normal-profile aileron was tested with a shorter cover plate (fig. 4). The partial seal of thin sheet rubber extended along the entire 1/4-inch nose gap and was continued across the small clearance gap at the outboard end. The inboard end of the aileron was unsealed because the orifice tubing prevented the use of an end seal (fig. 3).

The area of the vent gap between the aileron and the normal cover plate was 0.047 square foot. The leakage area

for the partially sealed normal-profile aileron was approximately 53 percent of that vent area, 51 percent at the inboard end, and 2 percent around the supports for the cover plate near the hinge line. The leakage area for the beveled aileron was 32 percent of the vent area, all at the inboard end, since the reduced overhang of the cover plate eliminated the necessity for additional support.

The tests were made through a Mach number range of 0.188 to 0.75, with a corresponding Reynolds number range of 5,000,000 to 13,800,000 based on a mean aerodynamic chord of 3.84 feet (fig. 6). The aileron angles varied from 15° to -15° by 2½° increments. For all the high-speed tests, angles of attack (table I) were selected to correspond to wing lift coefficients of -0.1, 0.1, and 0.3 at each Mach number with zero aileron deflection.

SYMBOLS

The symbols used in the presentation of the results are defined as follows:

A aspect ratio

C_L lift coefficient, L/qS_w

C_D drag coefficient, D/qS_w

$C_{m_{c/4}}$ pitching-moment coefficient, $M'/q\ (M.A.C.)\ S_w$

C_l rolling-moment coefficient, L'/qbS_w

C_n yawing-moment coefficient, N'/qbS_w

C_h aileron hinge-moment coefficient, $H_a/qb_a\overline{c_a}^2$

c wing chord

c_a aileron chord measured along airfoil chord line from hinge line of aileron to trailing edge of airfoil

$\overline{c_a}$ root-mean-square chord of the aileron aft of hinge line

b twice span of the semispan model

b_a aileron span

S_w twice area of the semispan model

L twice uncorrected lift of semispan model

D twice uncorrected drag of semispan model

M' twice uncorrected pitching moment (about 1/4c of M.A.C.) of semispan model

L' uncorrected rolling moment, due to aileron deflection, about longitudinal wind axis in plane of symmetry

N' uncorrected yawing moment, due to aileron deflection, about normal wind axis in plane of symmetry

H_a uncorrected moment of aileron about hinge axis

q dynamic pressure of the air stream, $1/2\rho V^2$, corrected for tunnel constriction and strut interference

M Mach number corrected for tunnel constriction and strut interference

α uncorrected angle of attack, degrees

δ_a aileron deflection relative to wing, degrees; positive when trailing edge is down

$\Delta\alpha$ mean change in angle of attack induced by the rolling velocity

C_{l_p} damping-moment coefficient, rate of change of rolling-moment coefficient C_l with $pb/2V$

$$\frac{\partial C_l}{\partial\left(\frac{pb}{2V}\right)}$$

$\frac{pb}{2V}$ tangent of wing-tip helix angle in roll

V true airspeed, feet per second

V_i indicated airspeed, feet per second

p rate of roll in flight, radians per second

S pressure coefficient, $(H-p_l)/q$

H total pressure

p_l local pressure on wing

ΔP coefficient of pressure difference across seal,

$$\frac{\text{pressure below seal - pressure above seal}}{q}$$

$$S_{upper}-S_{lower}$$

The parameters for aileron effectiveness are as follows:

$\left(\frac{\partial C_L}{\partial \alpha}\right)_{\delta_a}$ rate of change of lift coefficient with angle of attack, for a constant aileron deflection, degrees

$\left(\frac{\partial C_l}{\partial \delta_a}\right)_{\alpha}$ rate of change of rolling-moment coefficient with aileron deflection, for a constant angle of attack, degrees

$\left(\frac{\partial C_l}{\partial \alpha}\right)_{\delta_a}$ rate of change of rolling-moment coefficient (produced by the constant aileron deflection δ_a) with angle of attack, degrees

$\left(\frac{\partial C_h}{\partial \alpha}\right)_{\delta_a}$ rate of change of hinge-moment coefficient with angle of attack, for a constant aileron deflection, degrees

$\left(\frac{\partial C_h}{\partial \delta_a}\right)_{\alpha}$ rate of change of hinge-moment coefficient with aileron deflection, for a constant angle of attack, degrees

$\left(\frac{dC_h}{d\delta_a}\right)_{p}$ rate of change of hinge-moment coefficient with aileron deflection, during steady roll with equal up- and down-aileron deflections, degrees

RESULTS AND DISCUSSION

Reduction of Data

The data presented are based on the complete wing dimensions (fig. 1), and all of the data, except those showing the stick-force variation with $pb/2V$, represent the forces and

moments on the complete wing, assuming that only one aileron was deflected. None of the force data were corrected for strut interference or tunnel-wall effects. Consequently, the magnitude of the rolling-moment coefficient is approximately 10 percent too large. However, the correction for the angle of attack would have been nearly zero.

The dynamic pressures and Mach numbers were approximately corrected for tunnel-constriction effects and strut interference. This was accomplished by means of a velocity survey of the flow about the support strut with the wing removed and by determining (by an unpublished theoretical method) the constriction correction through the assumption of two-dimensional flow over the section of the wing containing the pressure orifices (fig. 1). The correction to the dynamic pressure for constriction by the model was less than 3 percent at the higher speeds and the corresponding Mach number correction was 2 percent. These constriction corrections are applicable only for speeds below that for the critical Mach number of the wing. The Mach number values given for speeds above the critical are probably a little low.

Variation of Lift

At all speeds the wing-alone tests, made with the aileron gaps sealed and faired smooth with putty, gave the same lift as obtained with the partially sealed normal-profile aileron (fig. 7). The angles of attack from the wing-alone tests (fig. 7) were used as representative of the characteristics for the particular lift coefficients (-0.1, 0.1, 0.3) presented for all the tests and results.

Static Characteristics of the Ailerons

Figures 8 to 25 present the variation of rolling-moment, hinge-moment, and yawing-moment coefficients with aileron deflection for each of the types tested. As an indication of the general scatter of the test points, the rolling-moment and hinge-moment coefficients are plotted in figure 26 for an aileron deflection of 10° and an angle of attack corresponding to a lift coefficient of 0.1 in terms of Mach number.

In order to determine the optimum rolling moment available from a completely sealed aileron, the normal-profile aileron was set at 10° and all the aileron gaps were sealed and faired smooth with putty. Figure 26 shows that at all

speeds the rolling moment obtained was practically the same as that produced by the same aileron when partially sealed. Consequently, the rolling moments for the partially sealed, normal-profile aileron may be used as a basis for comparison. Additional tests showed that a further reduction in the nose seal decreased the rolling moment.

Figures 8, 11, 17, and 20 show that in most instances the effect of increasing Mach number with the smooth wing surfaces was to increase slightly the rolling-moment coefficient produced by these ailerons, although the increase was not uniform and was generally much less than that predicted by the factor $1/\sqrt{1-M^2}$. The rolling-moment coefficient generally reached a maximum at a Mach number of 0.7 and decreased abruptly for Mach numbers greater than 0.725.

Although the unsealed beveled aileron was closely balanced for small deflections at low speeds (fig. 18), for large deflections the hinge moments were practically as great as for the partially sealed normal-profile aileron. Also, figure 18 shows an undesirable tendency of the close balance at low speeds to become an overbalance as the Mach number increases. The addition of the partial seal produced an even greater overbalance at high speeds (fig. 21).

The roughness at 0.10 chord on the wing decreased the variation of hinge-moment coefficient with speed (fig. 24). However, this does not necessarily mean that the variation in hinge-moment coefficient with Mach number for the smooth model was entirely due to the forward movement of transition. The effect of the roughness, in general, reduces the variation of all the wing characteristics with Mach number. Also, the drag measurements indicated there was no appreciable movement of the transition point until the compressibility effects became predominant at Mach numbers above the critical.

The leakage at the inboard end of all the partially sealed ailerons probably increased the hinge moments and reduced the aileron-deflection range over which $(\partial C_h/\partial \delta_a)_\alpha$ remained constant. (See reference 2.) However, as previously noted, this leakage was not large enough to change the rolling moment appreciably (fig. 26).

Aileron Control Characteristics

Figures 27 and 28 present the parameters which are

required to determine the hinge moment occurring during roll with small deflections of the partially sealed, normal-profile aileron. All the parameters were obtained for the region of 0° aileron deflection and 0° angle of attack. In addition, the theoretical value of $\left(\frac{\partial C_L}{\partial \alpha}\right)_{\delta_a} = \left[\frac{1}{\sqrt{1-M^2}} \frac{2\pi}{57.3} \left(\frac{A}{A+2}\right)\right]$ is compared with the experimental value (fig. 27). It is seen that for small aileron deflections at low angles of attack the effect of an increase in speed is to increase slightly $(\partial C_l/\partial \delta)_\alpha$ and decrease considerably the magnitude of $(\partial C_h/\partial \delta)_\alpha$. When the Mach number exceeds 0.725, both parameters are abruptly changed. In the appendix it is shown that the actual rate of change of hinge-moment coefficient during steady roll, with equal up- and down-aileron deflections, is given by

$$\left(\frac{dC_h}{d\delta_a}\right)_p = \left(\frac{\partial C_h}{\partial \delta_a}\right)_\alpha - 113 \left(\frac{\partial C_l}{\partial \delta_a}\right)_\alpha \left(\frac{\partial C_h}{\partial \alpha}\right)_{\delta_a}$$

for the airplane characteristics presented in table I. Consequently, figures 27 and 28 show that an increase of Mach number up to 0.7 will decrease the hinge-moment coefficient during roll. For example, an increase of Mach number from 0.3 to 0.7 would change $(dC_h/d\delta_a)_p$ from -0.00186 to -0.00096, equivalent to a decrease in hinge-moment coefficient of 48 percent. If the rolling velocity were neglected, the parameter $(\partial C_h/\partial \delta_a)_\alpha$ alone would determine the hinge-moment coefficient and, for the same Mach number increase, its value would change from -0.00227 to -0.00182, indicating only a 20-percent decrease of hinge-moment coefficient. However, since $(\partial C_h/\partial \alpha)_{\delta_a}$ varies considerably with angle of attack (fig. 29), the foregoing statements are true only for small aileron deflections (i.e., for rolling velocities such that $\Delta\alpha$, the mean change in angle of attack induced by the rolling velocity, remains near 0°). Consequently, when the data are available, cross plots similar to figure 29 should be made and the effect of roll upon hinge moment should be found directly from them. The variation of $\Delta\alpha$, as computed from table I and a cross plot from figure 11 for the rolling-moment variation with angle of attack, also is shown in figure 29.

Figures 30 and 31 present the aileron control characteristics corrected for the rolling velocity and for differences between the wind-tunnel and flight data. These aileron

control characteristics, in the form of stick force required to produce a given $pb/2V$, were computed for the characteristics shown in table I, which are essentially the same as those used in reference 1. The value of 0.55 for the damping-moment coefficient at small lift coefficients was used in reference 1 to correct for the differences (including a tunnel-wall correction of approximately 10 percent, the effect of elasticity in the wing-aileron system, and the reduced response due to sideslip) between the wind-tunnel data and actual rolling moment available in flight. The same value of the damping-moment coefficient was used in this report, since the low-speed rolling-moment curves obtained with the partial seal agreed closely with those given in reference 1. The mean change in angle of attack induced by the rolling velocity $\Delta\alpha$, as given by the equation in table I, was assumed to be the change at a point 0.10 of the aileron span from the inboard end. (See reference 3.) The rolling-moment and hinge-moment coefficients, for equal up- and down-aileron deflections, were corrected for rolling velocity by using the coefficients corresponding to the mean angle of attack occurring during roll (e.g., see fig. 29). Figure 30 is for a Mach number of 0.7 and a lift coefficient of 0.1, with a dynamic pressure of 337 pounds per square foot (table I). These conditions correspond to flight at an altitude of 19,900 feet with a true airspeed of 496 miles per hour and an indicated airspeed of 374 miles per hour. For a direct comparison of the effects of Mach number, the curves in figure 31 were obtained for a Mach number of 0.3 with the same lift coefficient of 0.1 and dynamic pressure of 337 pounds per square foot. Also included in figures 30 and 31 are the static aileron control characteristics for the partially sealed, normal-profile aileron, computed by neglecting the rolling velocity.

For small deflections the efficiency ($pb/2V$ produced by a given stick force) for the partially sealed normal-profile aileron increased with Mach number in agreement with the previous computations from the aileron parameters. However, for aileron deflections greater than 6°, (corresponding to a stick travel of 3.2 in.), the efficiency decreased as the Mach number increased even though the static efficiency (neglecting the rolling velocity) increased with Mach number (figs. 30 and 31). This occurred because the correction for the rolling velocity, which generally increased the efficiency in roll, actually decreased the efficiency for aileron deflections greater than 6° at the higher Mach number (fig. 30). As before, the increase in efficiency during roll was due to

the negative value of $(\partial C_h/\partial\alpha)_{\delta_a}$ as shown in the appendix. However, the decrease in efficiency during roll at the higher Mach number was due to the variation of $(\partial C_h/\partial\alpha)_{\delta_a}$ and $(\partial C_l/\partial\alpha)_{\delta_a}$ with angle of attack. These variations at a Mach number of 0.7 were such that the $\Delta\alpha$ resulting from aileron deflections greater than 6° ($pb/2V > 0.042$) actually increased the hinge moment and decreased the rolling moment. (See fig. 29.) The value of $pb/2V$ attained for a given aileron deflection (or stick travel) was less for the condition of steady roll than for the case where the rolling velocity was neglected because of the variation of $(\partial C_l/\partial\alpha)_{\delta_a}$ with angle of attack. Figures 30 and 31 show that the effect of $(\partial C_l/\partial\alpha)_{\delta_a}$ was much greater at the higher Mach number and the larger aileron deflections. With the exception of the large aileron deflections at high Mach numbers, the values of $(\partial C_l/\partial\alpha)_{\delta_a}$ were relatively small, so that during roll the change in efficiency would be mainly due to $(\partial C_h/\partial\alpha)_{\delta_a}$, as is assumed in the appendix.

Figures 30 and 31 show that the beveled aileron became overbalanced during roll as the Mach number increased. In addition, since the available rolling moments were less for the beveled aileron (fig. 20), the maximum value of $pb/2V$ was much less than that obtained by the normal-profile aileron and the stick forces were greater for the higher values of $pb/2V$. (See figs. 30 and 31.)

It is important to note that, although any change in lift-curve slope would affect the damping-moment coefficient, the value of 0.55 was used for all the preceding computations since the actual change in damping-moment coefficient could not be determined. The lift-curve slope increased 44 percent when the Mach number increased from 0.3 to 0.7 (fig. 27). However, the lift-curve slope of the tip portion of the wing, containing the aileron, would be predominant in determining the damping-moment coefficient and also, at high speeds, the lift-curve slope with the ailerons deflected was different from that with the ailerons neutral. In addition, a Mach number increase may increase the damping-moment coefficient due to other causes, such as an increased wing twist. (See figs. 33 to 35.) In view of the above reasons, no adjustment of the damping-moment coefficient was made for the beveled ailerons, which decreased the lift-curve slope 3.7 percent (fig. 7). The effect of a small decrease, say 10

percent, in the damping-moment coefficient could be approximated by increasing the $pb/2V$ by 10 percent for the given stick force.

The general indication from these tests was that (in the aileron characteristics) no severe compressibility effects would be encountered until a Mach number of 0.725 was exceeded. Figures 27 and 28 indicate that the first slight effects of the compression shock may become noticeable when the Mach number exceeds 0.7.

Pitching Moment Induced by Ailerons

The pitching-moment increment acting on each wing tip would tend to twist the wing so as to decrease the rolling moment, and the speed at which the rolling moment accompanying the elastic twist of the wing nullifies the rolling moment produced by the ailerons is defined as the aileron reversal speed. In order to provide data necessary to determine the effect of Mach number upon the aileron reversal speed, the increments of pitching-moment coefficient produced by aileron deflection were plotted (figs. 32 to 35). These increments are based on the pitching moment taken about the quarter point of the mean aerodynamic chord. They increased rapidly with Mach number until they reached a maximum value at a Mach number of 0.725, and then they decreased abruptly.

Balance Pressures

Figures 36 to 38 show the balance pressures under the cover plates. The coefficient ΔP is a measure of the pressure difference across the balance seal. It was measured at the chord line containing the wing pressure orifices (fig. 1). Figures 36 and 37 show the variation of ΔP, at constant Mach numbers, with aileron angle for the partially sealed normal-profile aileron and for the beveled aileron, respectively. Figure 38 provides for comparisons of the effects of a shorter cover plate on the partially sealed normal-profile aileron, of roughness at 0.10 wing chord on the partially sealed beveled aileron, and of an additional leakage area of 2 percent of the vent area in the seal of the partially sealed beveled aileron. The partially sealed beveled aileron (fig. 37) developed higher balance pressures than did the partially sealed normal-profile aileron (fig. 36). However, comparison of figures 36 and 38 shows that the balance

pressures became approximately the same when equal leakage area was present in both nose seals. With this additional 2-percent leakage area, the hinge moment of the beveled aileron was increased approximately 10 percent at a 15° aileron deflection, but the rolling moment and yawing moment were unaffected.

The spanwise variation of the pressure coefficients acting above and below the seal is shown in figures 39 and 40 for the partially sealed normal-profile aileron and the partially sealed beveled aileron, respectively. Because of the large leakage area at the inboard end, the pressure difference was decreased over a considerable portion of the nose balance. Also, the velocities induced by the support strut at the inboard end of the aileron probably contributed something toward this decrease. However, the data indicate that the leakage at the inboard end had no appreciable effect on the balance pressures presented in figures 36 to 38, since ΔP was measured at a position 0.45 of the aileron span from the inboard end.

Pressure Distributions

Figures 41 to 49 present the pressure distributions for the partially sealed normal-profile aileron and the partially sealed beveled aileron for deflections of 0°, 10°, and -10°. All of the curves for a Mach number of 0.3 or more are for the angles of attack corresponding to a lift coefficient of 0.1 for the wing alone (fig. 7 and table I). The values of S_{cr}, the pressure coefficient for which the local velocity over the wing is equal to the local velocity of sound at the corresponding free-stream Mach number defined as M_{cr}, are also shown.

Figures 50 and 51 provide for a direct comparison of the pressure distributions for aileron deflections of 0° and 10°, respectively, at an angle of attack corresponding to a lift coefficient of 0.1. Figure 51 indicates that, due to the air flow through the nose gap, there was considerable separation over the upper surface of the unsealed normal-profile aileron with a 10° deflection. This separation reduced the section lift and the resulting rolling moment. However, with a 0° aileron deflection, the pressure difference across the nose gap was small, and the flow through the gap was not sufficient to cause appreciable separation (fig. 50).

A critical Mach number (M_{cr}) of 0.67, corresponding to the S_{cr} obtained from the peak-pressure measurements (fig. 41 and reference 4), was indicated for the wing at a lift coefficient of 0.1. It is important to note that this critical Mach number is merely the speed that must be exceeded in order to obtain the conditions necessary for the formation of a compression shock. Figure 11 shows that the rolling-moment coefficient had not decreased even at a Mach number of 0.725, indicating that the critical Mach number was exceeded by 8 percent before the compression shock seriously affected the action of the aileron. The wing itself was more immediately affected since the lift-curve slope decreased rapidly after a Mach number of 0.7 was exceeded (fig. 27).

The pressure distribution indicates a compression shock between 60- and 65-percent chord at a Mach number of 0.7. Consequently, the abrupt change of the aerodynamic forces and moments on the model, generally occurring at or beyond a Mach number of 0.725, would be expected.

CONCLUDING REMARKS

These tests have indicated that a further study of hinge-moment coefficients at high speeds is advisable, since there was evidence that ailerons closely balanced at low speeds might become overbalanced as the Mach number increased. This was especially true for the beveled ailerons. The tests showed that no serious adverse compressibility effects were encountered until the critical Mach number (0.67) was exceeded by at least 8 percent.

Ames Aeronautical Laboratory,
National Advisory Committee for Aeronautics,
Moffett Field, Calif.

APPENDIX

Analysis of Aileron Hinge Moment during Response

If the rolling velocity is assumed constant and there is no sideslip or yawing,

$$\Delta C_l = \frac{\partial C_l}{\partial\left(\frac{pb}{2V}\right)}\left(\frac{pb}{2V}\right) = C_{l_p}\left(\frac{pb}{2V}\right)$$

However, this expression will generally be a good approximation even with the sideslip occurring with locked rudder at a constant rolling velocity, provided that the value of $pb/2V$ is decreased by a theoretical allowance for the effect of sideslip. Consequently,

$$\left(\frac{pb}{2V}\right) \approx \frac{\Delta C_l}{C_{l_p}}$$

The magnitude of the change in angle of attack induced by the rolling velocity at distance $yb/2$ from the axis of rotation is

$$|\Delta\alpha| = \tan^{-1} y\,\frac{pb}{2V}$$

When $yb/2$ is a mean-wing-span location determined from the load distribution (reference 3), then $\Delta\alpha$ may be used as the mean change in angle of attack for the entire wing. The value of $yb/2$ is determined by whether the effect of the rolling velocity on the rolling moment or the hinge moment is being considered. However, since the effect of the rolling velocity on the rolling moment is generally small, the same value of $yb/2$ which is computed for the hinge-moment correction may be used. Since the values of $pb/2V$ are small,

$$|\Delta\alpha| \approx 57.3y\,\frac{pb}{2V} \approx 57.3y\,\frac{\Delta C_l}{C_{l_p}}, \quad \text{degrees}$$

If it is assumed that the aileron rolling-moment coefficient varies linearly, then for one aileron alone

$$C_l \approx \left(\frac{\partial C_l}{\partial \delta_a}\right)_\alpha \delta_a$$

since $\Delta\alpha$ is always small and $(\partial C_l/\partial\alpha)_{\delta_a}$ is also small except for large aileron deflections at high speeds. Then for equal up- and down-aileron deflections, the total rolling-moment coefficient available during roll is

$$\Delta C_l \approx 2\left(\frac{\partial C_l}{\partial \delta_a}\right)_\alpha |\delta_a|$$

Then

$$|\Delta\alpha| \approx 57.3y \left[\frac{2\left(\frac{\partial C_l}{\partial \delta_a}\right)_\alpha |\delta_a|}{C_{l_p}}\right], \text{ degrees}$$

or

$$\left|\frac{\Delta\alpha}{\delta_a}\right| \approx 2\left(\frac{57.3y}{C_{l_p}}\right)\left(\frac{\partial C_l}{\partial \delta_a}\right)_\alpha$$

If it is assumed that the aileron hinge-moment coefficient varies linearly, then during roll the resulting total hinge-moment ΔC_h is

$$\left(\frac{\partial C_h}{\partial \delta_a}\right)_\alpha (\delta_a)_{down} + \left(\frac{\partial C_h}{\partial \alpha}\right)_{\delta_a} (\alpha - |\Delta\alpha|) - \left(\frac{\partial C_h}{\partial \delta_a}\right)_\alpha (\delta_a)_{up} - \left(\frac{\partial C_h}{\partial \alpha}\right)_{\delta_a} (\alpha + |\Delta\alpha|)$$

Or, for equal up- and down-aileron deflections, the actual total hinge-moment coefficient during roll is

$$\Delta C_h = 2\left(\frac{\partial C_h}{\partial \delta_a}\right)_\alpha |\delta_a| - 2\left(\frac{\partial C_h}{\partial \alpha}\right)_{\delta_a} |\Delta\alpha|$$

$$= \left[1 - \left|\frac{\Delta\alpha}{\delta_a}\right| \frac{\left(\frac{\partial C_h}{\partial \alpha}\right)_{\delta_a}}{\left(\frac{\partial C_h}{\partial \delta_a}\right)_\alpha}\right] \left(\frac{\partial C_h}{\partial \delta_a}\right)_\alpha (2\,|\delta_a|)$$

$$= \left[1 - 2(57.3y)\,\frac{\left(\frac{\partial C_l}{\partial \delta_a}\right)_\alpha}{C_{l_p}} \frac{\left(\frac{\partial C_h}{\partial \alpha}\right)_{\delta_a}}{\left(\frac{\partial C_h}{\partial \delta_a}\right)_\alpha}\right] \left(\frac{\partial C_h}{\partial \delta_a}\right)_\alpha (2\,|\delta_a|)$$

where α and δ_a are measured in degrees.

This expression for the actual total hinge-moment coefficient shows the effect of each parameter upon the stick force occurring during roll (reference 5).

The actual rate of change of hinge-moment coefficient with equal up- and down-aileron deflections could be written as

$$\frac{\Delta C_h}{2|\delta_a|} = \left(\frac{dC_h}{d\delta_a}\right)_p = \left[\left(\frac{\partial C_h}{\partial \delta_a}\right)_\alpha - 2\left(\frac{57.3y}{C_{l_p}}\right)\left(\frac{\partial C_l}{\partial \delta_a}\right)_\alpha \left(\frac{\partial C_h}{\partial \alpha}\right)_{\delta_a}\right]$$

which is equivalent to

$$\left(\frac{dC_h}{d\delta_a}\right)_p = \left(\frac{\partial C_h}{\partial \delta_a}\right)_\alpha + \left(\frac{\partial C_h}{\partial \alpha}\right)_{\delta_a}\left(\frac{\partial \Delta\alpha}{\partial \delta_a}\right)_p$$

since the value of $(\partial\Delta\alpha/\partial\delta_a)_p$ due to steady roll would be given by

$$\left(\frac{\partial \Delta\alpha}{\partial \delta_a}\right)_p = -2\left(\frac{57.3y}{c_{l_p}}\right)\left(\frac{\partial c_l}{\partial \delta_a}\right)_\alpha$$

the negative sign being correct, since an aileron deflection of $\pm\delta_a$ is accompanied by an induced angle-of-attack change of $\mp\Delta\alpha$ at all ordinary conditions.

For the values given in table I, the expression for the actual rate of change of hinge-moment coefficient during roll with equal up- and down-aileron deflection becomes

$$\left(\frac{dc_h}{d\delta_a}\right)_p = \left[\left(\frac{\partial c_h}{\partial \delta_a}\right)_\alpha - 113\left(\frac{\partial c_l}{\partial \delta_a}\right)_\alpha \left(\frac{\partial c_h}{\partial \alpha}\right)_{\delta_a}\right]$$

It is obvious that negative values of $(\partial c_h/\partial\alpha)_{\delta_a}$ will be favorable, since they will decrease the hinge moments. When $(\partial c_h/\partial\alpha)_{\delta_a} = \frac{1}{113}\frac{(\partial c_h/\partial\delta_a)_\alpha}{(\partial c_l/\partial\delta_a)_\alpha}$, the resulting hinge moment during roll will be zero, and when $(dc_h/d\delta_a)_p$ is positive, the ailerons will be overbalanced in roll.

It is to be noted that generally the parameters are linear only for small aileron deflections and low angles of attack. The parameter $(\partial c_h/\partial\alpha)_{\delta_a}$ sometimes even changes algebraic value with the small angle-of-attack variation $(\Delta\alpha)$ induced by the rolling velocity. (See fig. 29 and reference 5.)

REFERENCES

1. Rogallo, F. M., and Lowry, John G.: Wind-Tunnel Development of Ailerons for the Curtiss XP-60 Airplane. NACA ACR, Sept. 1942.

2. Rogallo, F. M., and Lowry, John G.: Resumé of Data for Internally Balanced Ailerons. NACA RB, March 1943.

3. Sears, Richard I.: Application of Balancing Tabs to Ailerons. NACA RB, June 1942.

4. Von Kármán, Th.: Compressibility Effects in Aerodynamics. Jour. of the Aero. Sci., vol. 8, no. 9, July 1941, pp. 337-356.

5. Gates, S. B., and Irving, H. B.: An Analysis of Aileron Performance. Rep. No. B.A. 1624, British R.A.E., July 1940.

TABLE I.- DATA FOR $\frac{pb}{2V}$ COMPUTATIONS

[α corresponding to C_L given on curves]

M	0.188-0.3	0.5	0.6	0.65	0.675	0.7	0.725	0.75
$\alpha_{C_L=-0.1}$	-1.7	-1.7	-1.8	-1.5	-1.5	-1.6	-1.9	-3.2
$\alpha_{C_L=0.1}$	.7	.5	.3	.3	.3	.1	0	0
$\alpha_{C_L=0.3}$	3.2	2.9	2.4	2.2	2.0	1.8	1.7	2.7

Wing loading = 33.7 lb/ft^2

Maximum stick travel = ± 8 in.

Maximum aileron deflection = $\pm 15^\circ$

Aileron differential = 1 : 1

Stick travel (ft)/aileron deflection (rad) = 2.55 ft

Aileron span $\times$ $(\text{chord}_{rms})^2 = b_a \bar{c}_a^2$ = 5.60 ft^3

Stick force = 2.20 $q\Delta C_h$ lb

Damping coefficient = $C_{l_p} = \dfrac{dC_l}{\partial\left(\frac{pb}{2V}\right)} = 0.55$

$\therefore \dfrac{pb}{2V} = \dfrac{\Delta C_l}{0.55}$

Angle change induced by roll = $\Delta\alpha$ = $0.541\left(\frac{pb}{2V}\right)$

CHARACTERISTICS OF THE 0.531- SCALE MODIFIED XP-60 WING

AREA (S)---- 76.98 ft²
SPAN (b)---- 22 ft
ASPECT RATIO-6.28
TAPER RATIO--3:1
WING SECTION (NO TWIST)
ROOT--NACA 66,2-118
TIP---NACA 66,2X-116
AILERONS
SPAN----- 4.51 ft
CHORD-.15 LOCAL WING CHORD
BALANCE-.60 OF AILERON CHORD
AILERON $S_{PAN} \times (CHORD_{rms})^3 = 0.838 ft^3$

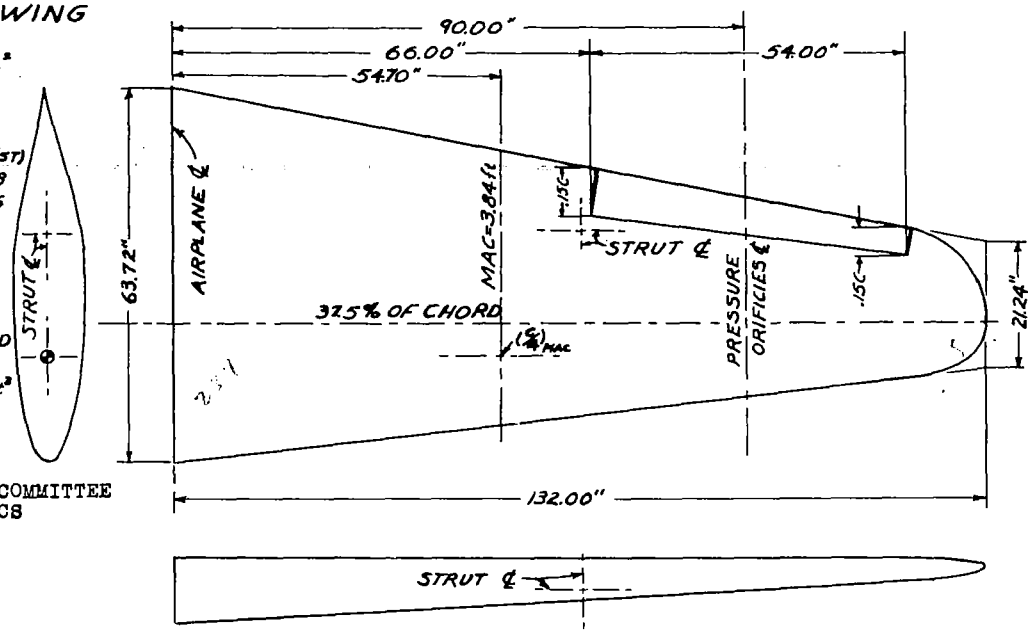

NATIONAL ADVISORY COMMITTEE FOR AERONAUTICS

FIGURE 1.- DIMENSIONS OF MODEL

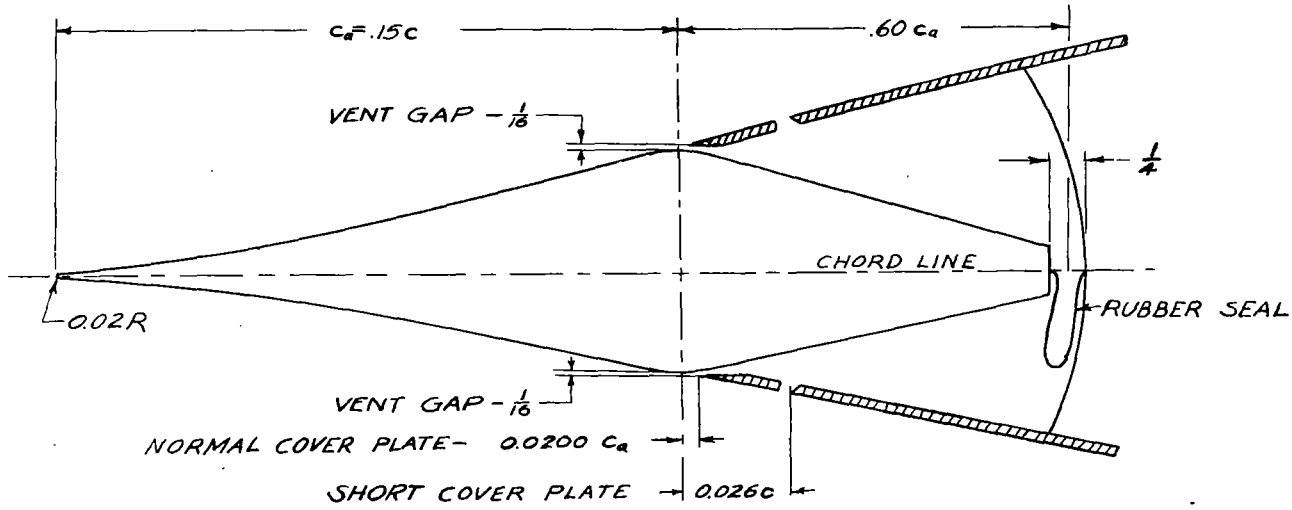

FIGURE 4- NORMAL-PROFILE AILERON

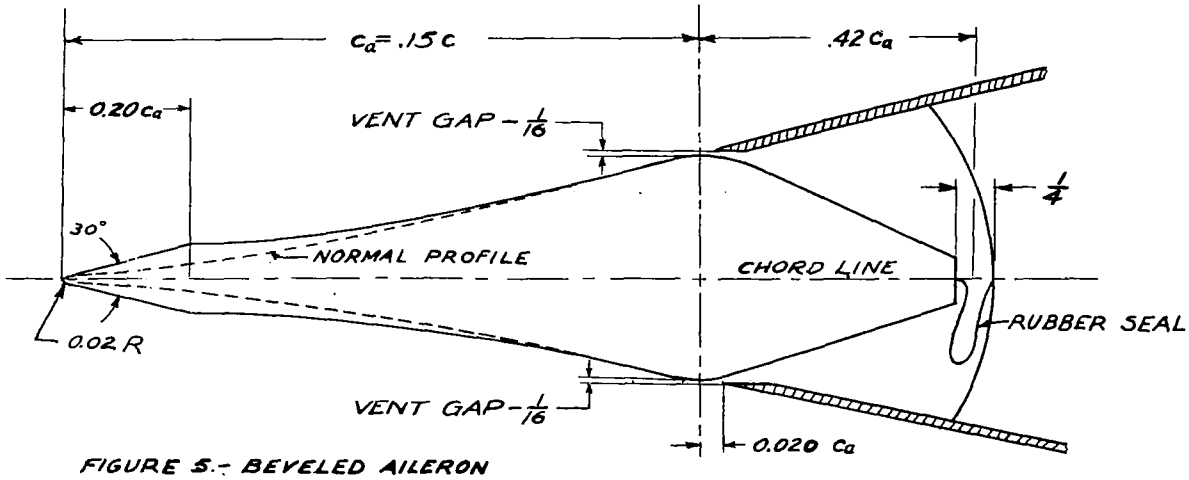

FIGURE 5.- BEVELED AILERON

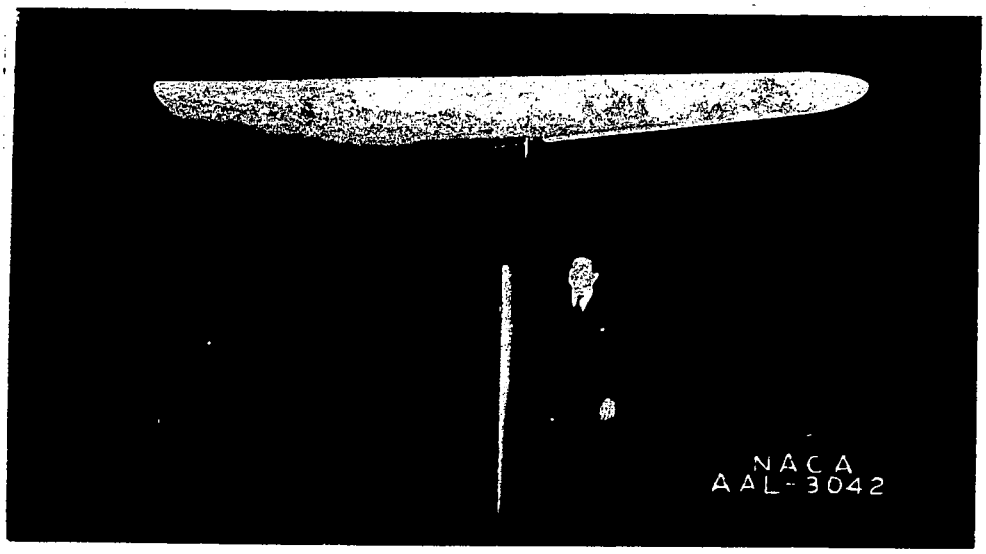

Figure 2.- Tapered wing model mounted in 16-foot wind tunnel.

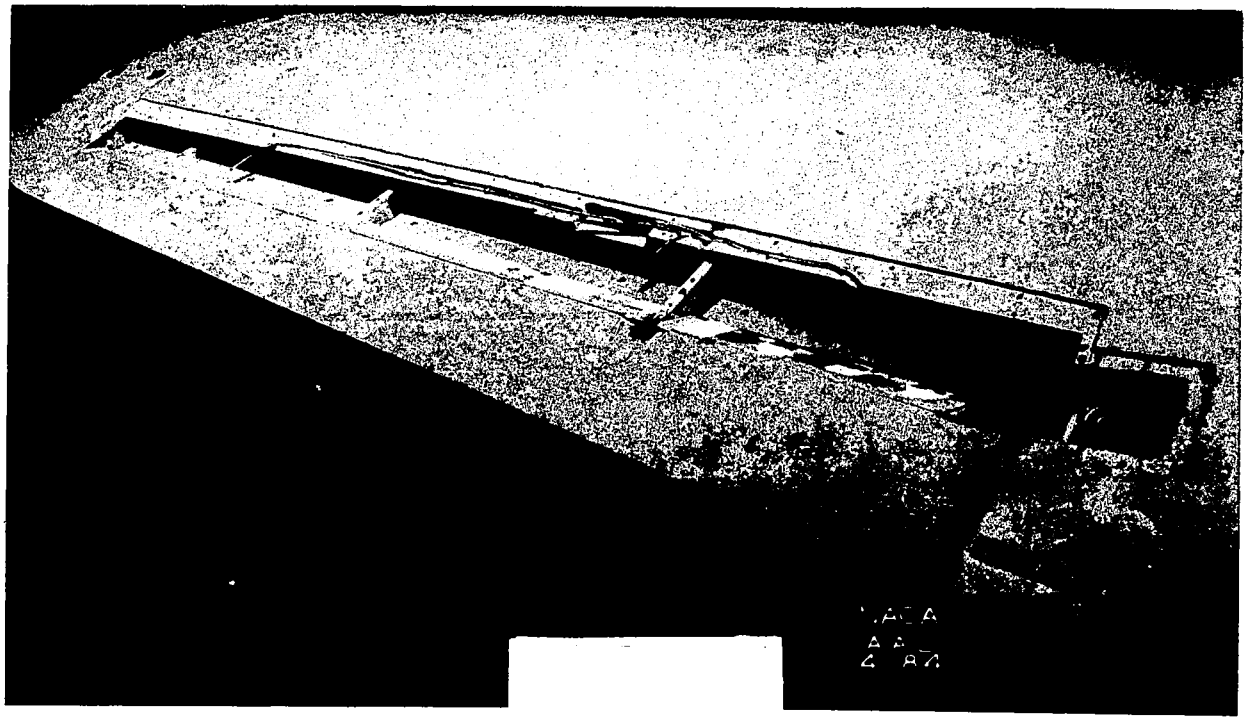

Figure 3.- View of aileron with cover plate removed.

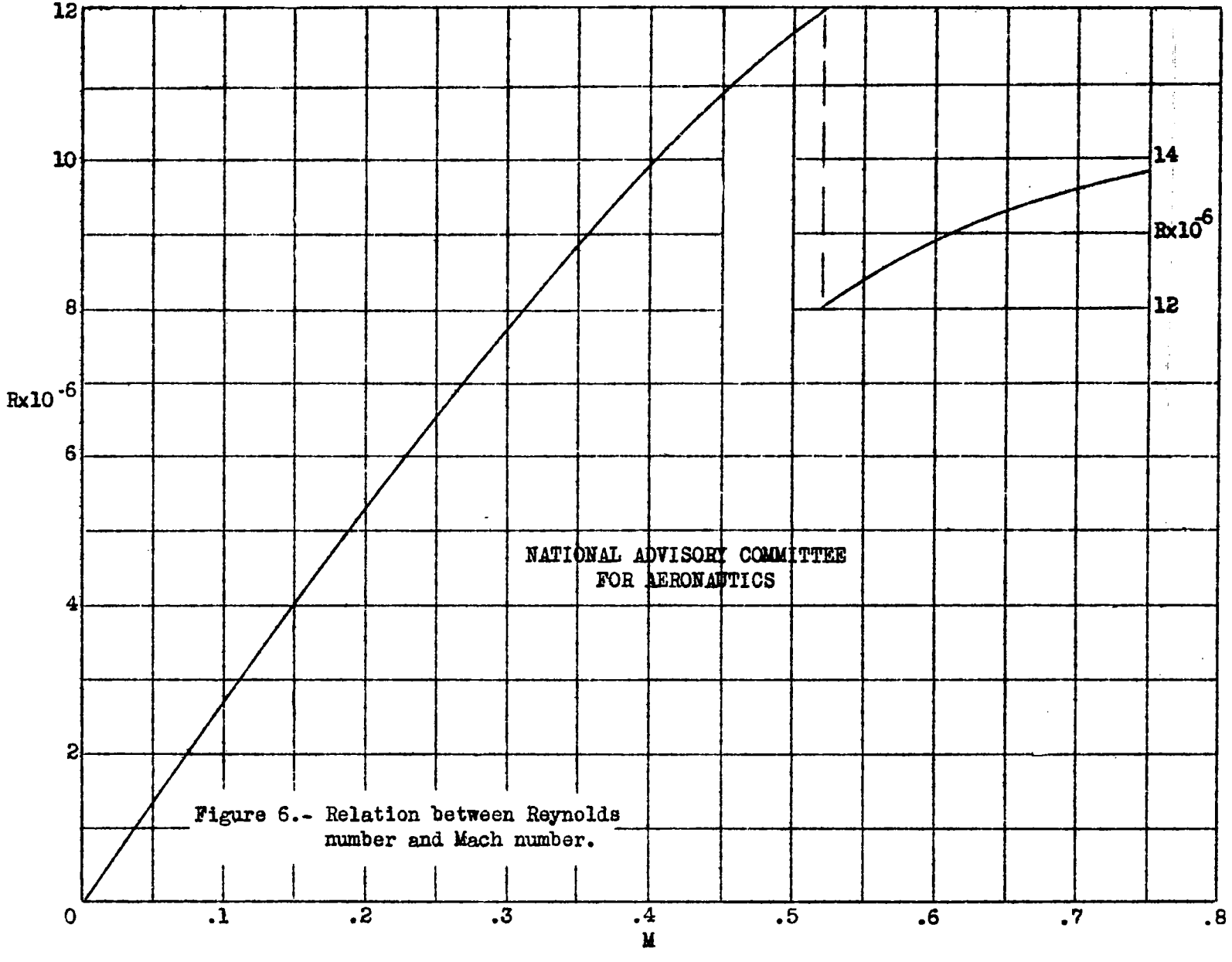

Figure 6.- Relation between Reynolds number and Mach number.

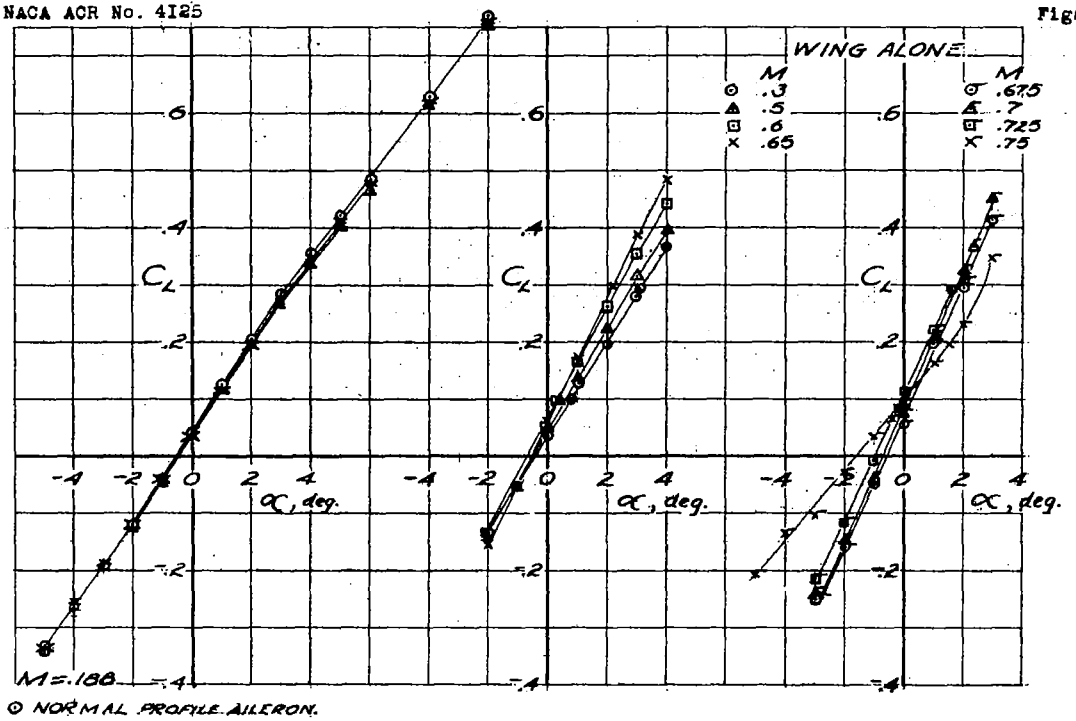

FIGURE 7.— VARIATION OF LIFT COEFFICIENT WITH ANGLE OF ATTACK $\delta_a = 0°$

NATIONAL ADVISORY COMMITTEE FOR AERONAUTICS

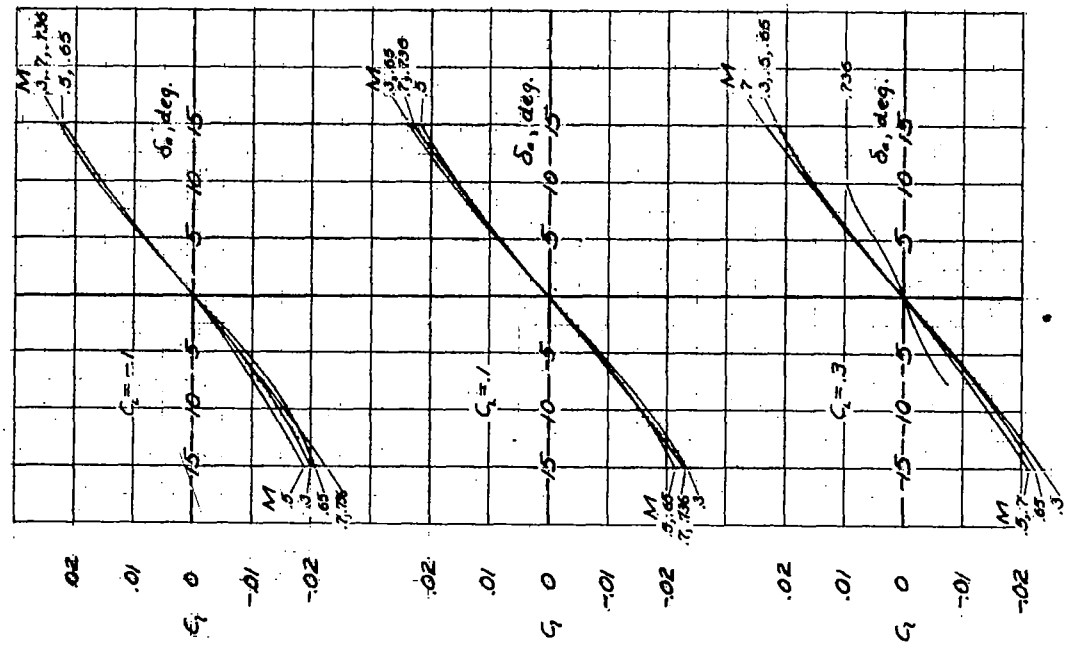

FIGURE 8.- VARIATION OF ROLLING-MOMENT COEFFICIENT WITH AILERON DEFLECTION FOR UNSEALED NORMAL-PROFILE AILERON

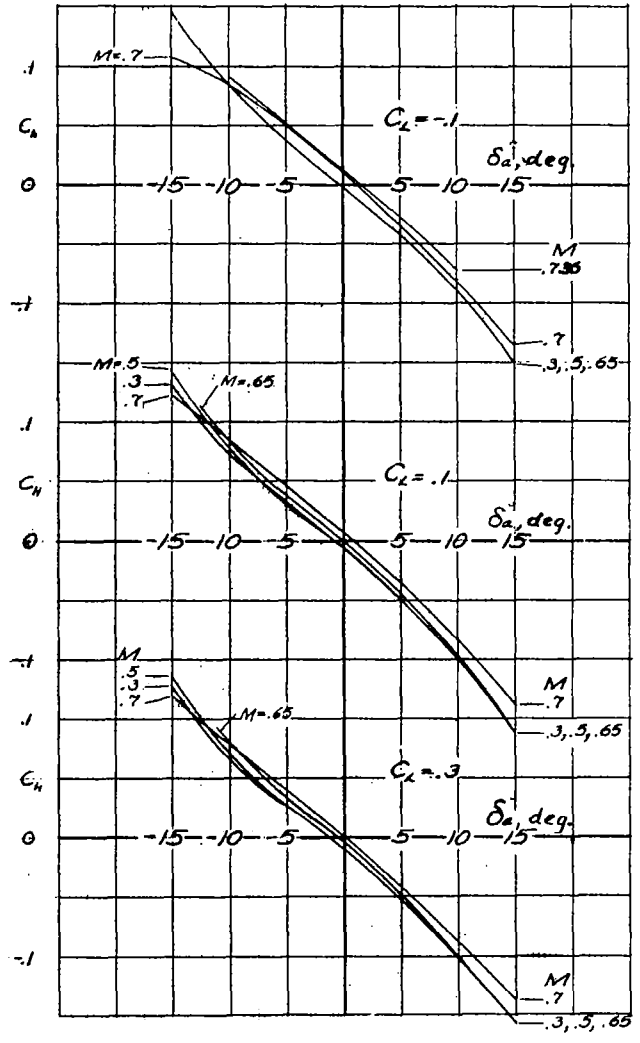

FIGURE 9-VARIATION OF HINGE-MOMENT COEFFICIENT WITH AILERON DEFLECTION FOR UNSEALED NORMAL-PROFILE AILERON

NATIONAL ADVISORY COMMITTEE FOR AERONAUTICS

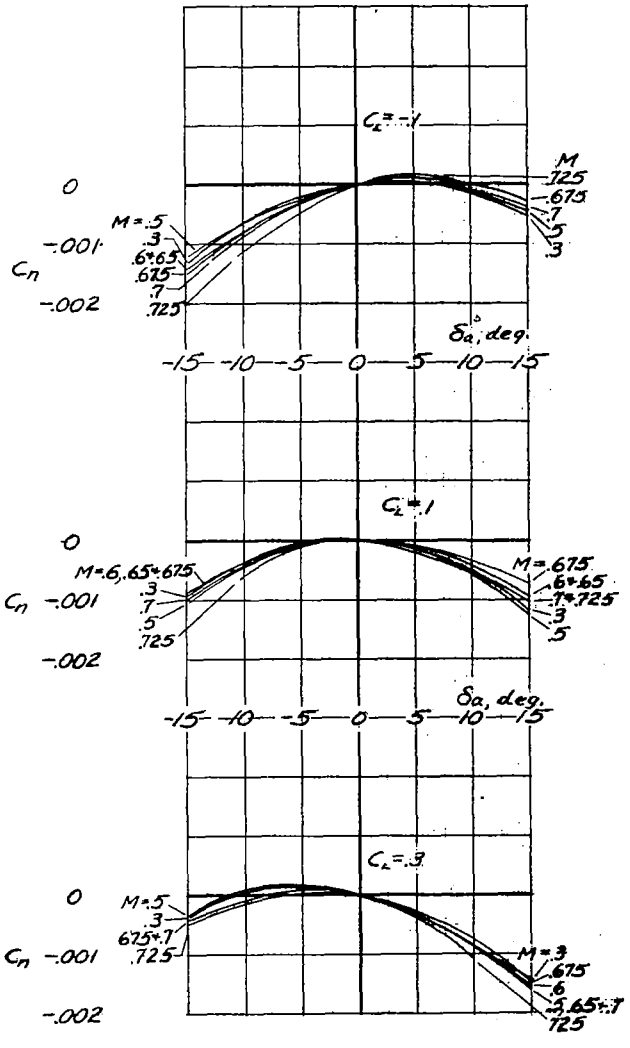

FIGURE 10-VARIATION OF YAWING-MOMENT COEFFICIENT WITH AILERON DEFLECTION FOR UNSEALED NORMAL-PROFILE AILERON

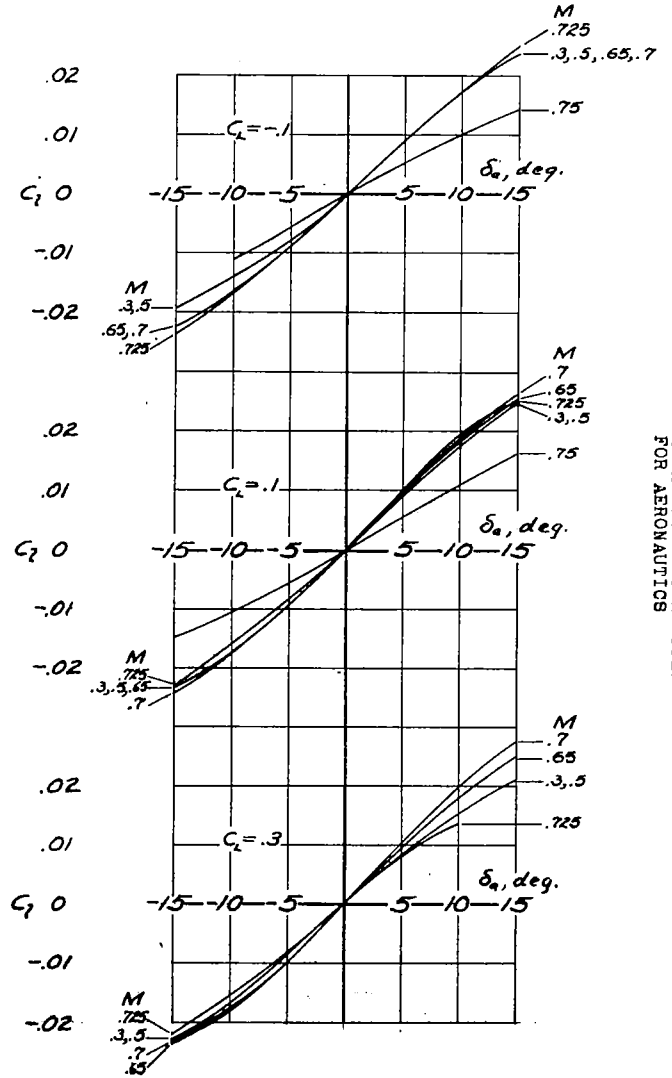

FIGURE 11 - VARIATION OF ROLLING-MOMENT COEFFICIENT WITH AILERON DEFLECTION FOR PARTIALLY-SEALED NORMAL-PROFILE AILERON

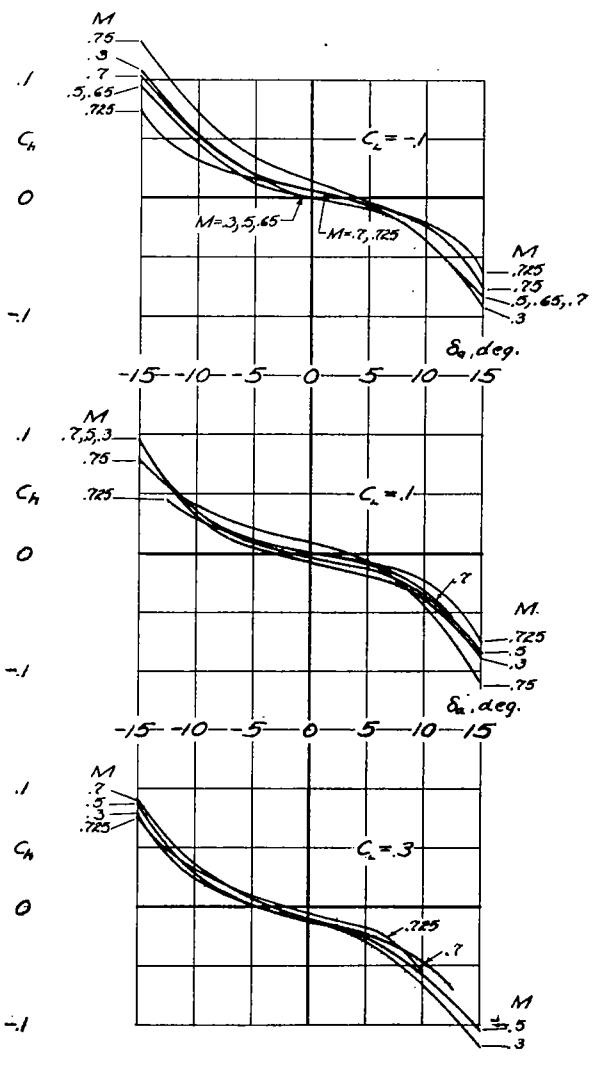

FIGURE 12 - VARIATION OF HINGE-MOMENT COEFFICIENT WITH AILERON DEFLECTION FOR PARTIALLY SEALED NORMAL-PROFILE AILERON

NATIONAL ADVISORY COMMITTEE FOR AERONAUTICS

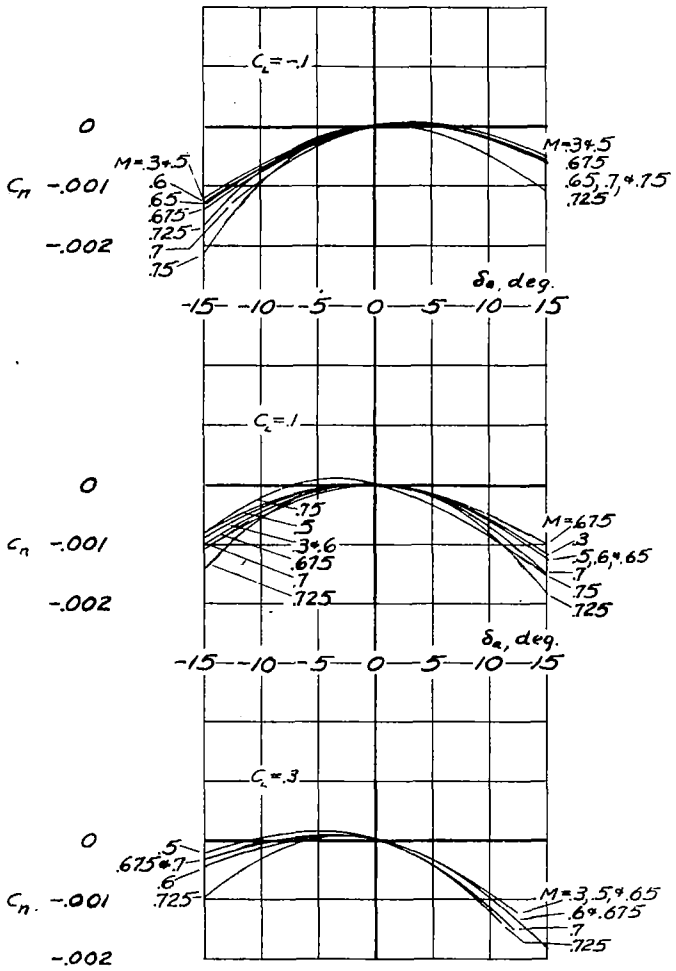

FIGURE 13 - VARIATION OF YAWING-MOMENT COEFFICIENT WITH AILERON DEFLECTION FOR PARTIALLY SEALED NORMAL-PROFILE AILERON

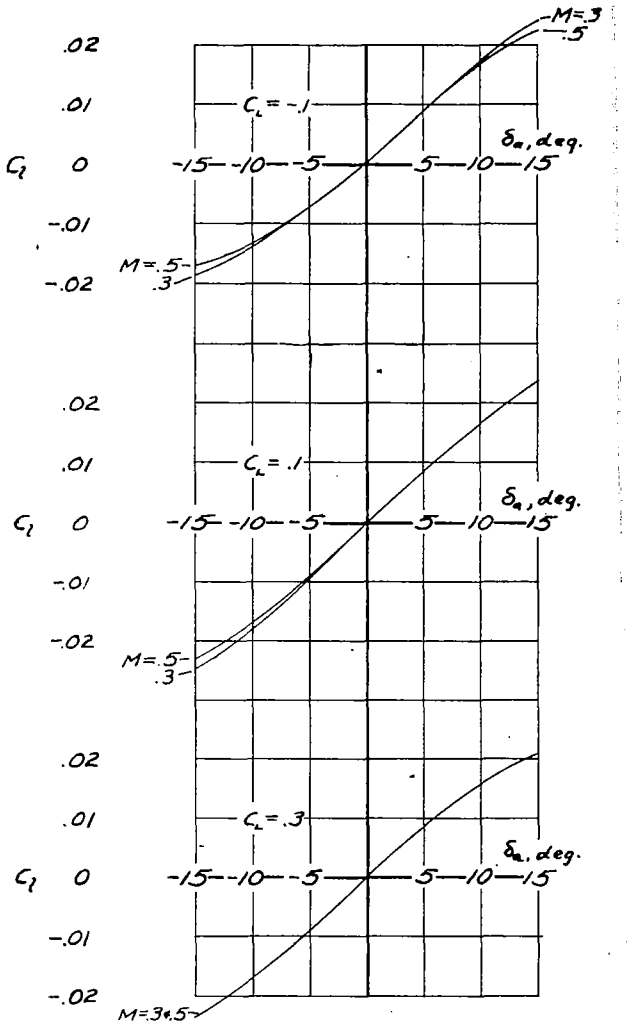

FIGURE 14 - VARIATION OF ROLLING-MOMENT COEFFICIENT WITH AILERON DEFLECTION FOR PARTIALLY SEALED NORMAL-PROFILE AILERON WITH SHORT COVER PLATE

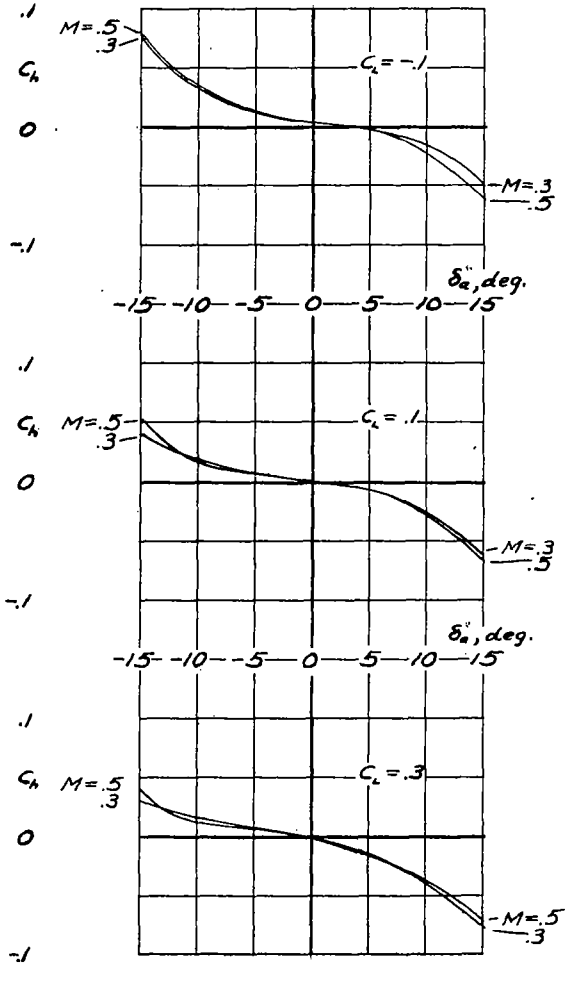

FIGURE 15- VARIATION OF HINGE-MOMENT COEFFICIENT WITH AILERON DEFLECTION FOR PARTIALLY SEALED NORMAL-PROFILE AILERON WITH SHORT COVER PLATE

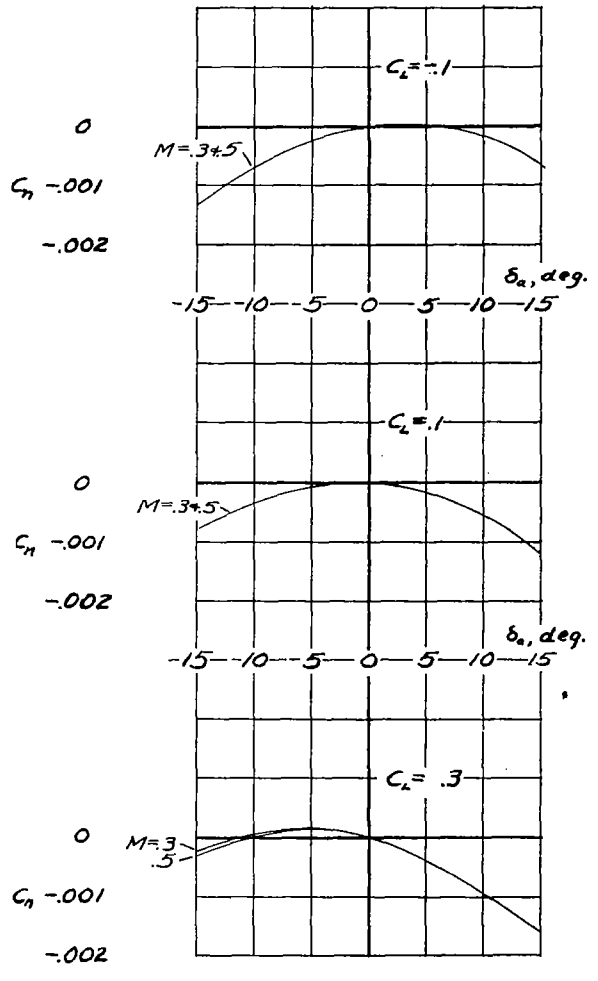

FIGURE 16 -VARIATION OF YAWING-MOMENT COEFFICIENT WITH AILERON DEFLECTION FOR PARTIALLY SEALED NORMAL-PROFILE AILERON WITH SHORT COVER PLATE

NATIONAL ADVISORY COMMITTEE FOR AERONAUTICS

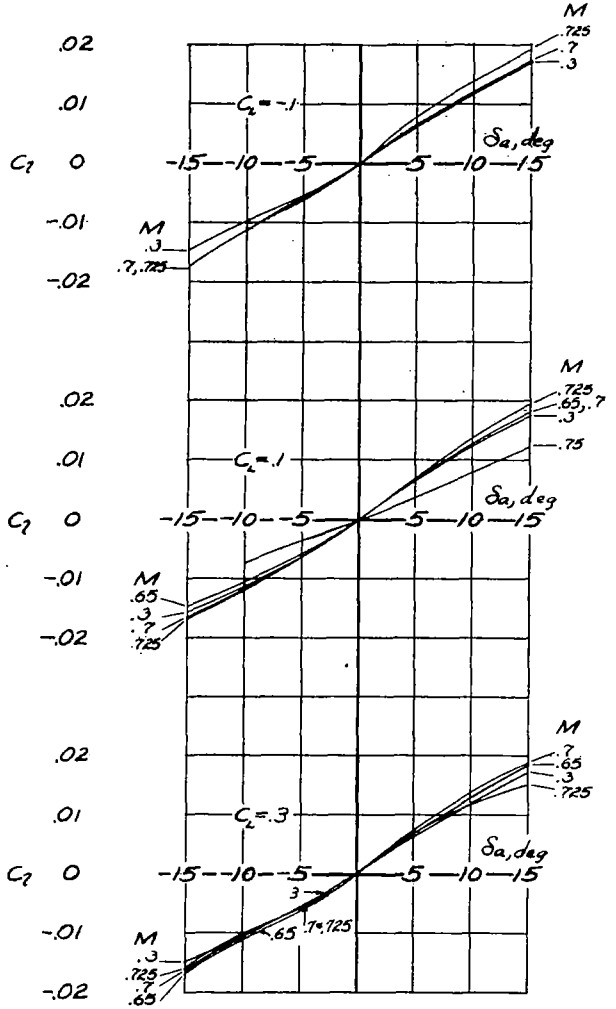

FIGURE 17 - VARIATION OF ROLLING-MOMENT COEFFICIENT WITH AILERON DEFLECTION FOR UNSEALED BEVELED AILERON

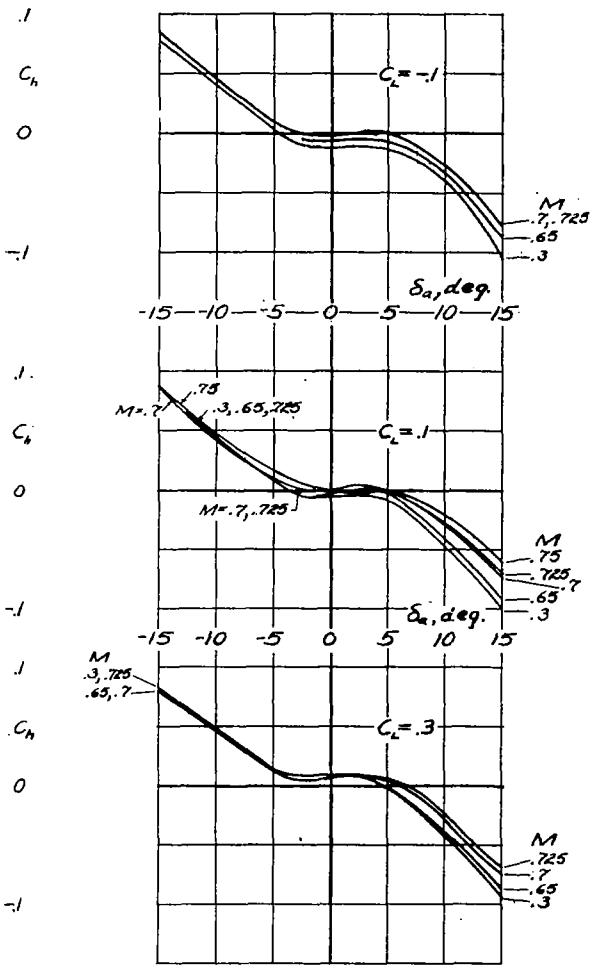

FIGURE 18 - VARIATION OF HINGE-MOMENT COEFFICIENT WITH AILERON DEFLECTION FOR UNSEALED BEVELED AILERON

NATIONAL ADVISORY COMMITTEE FOR AERONAUTICS

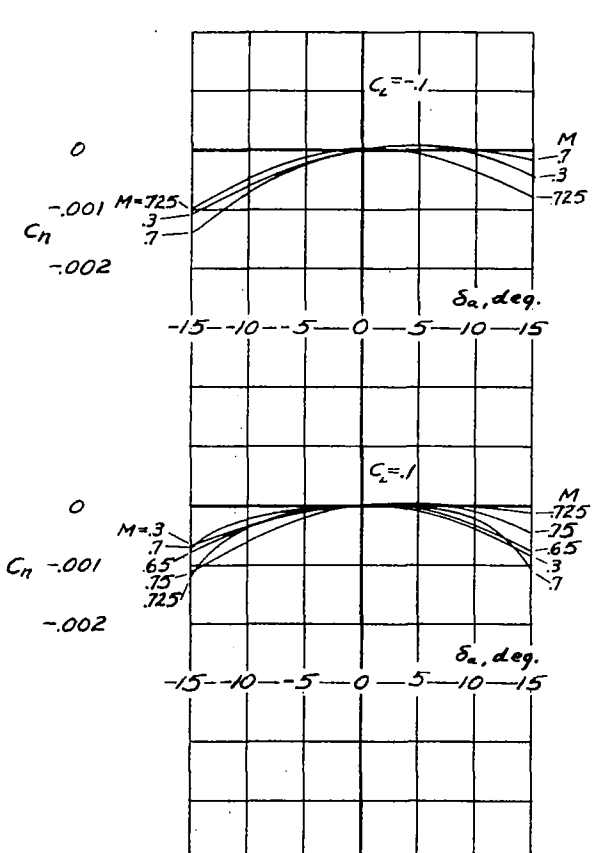

FIGURE 19- VARIATION OF YAWING-MOMENT COEFFICIENT WITH AILERON DEFLECTION FOR UNSEALED BEVELED AILERON

NATIONAL ADVISORY COMMITTEE FOR AERONAUTICS

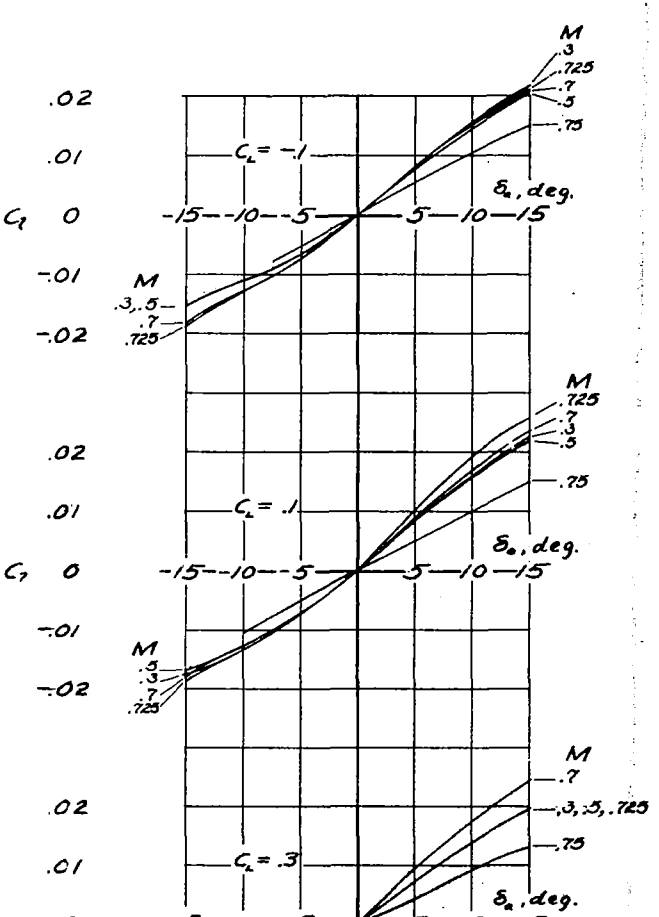

FIGURE 20 - VARIATION OF ROLLING-MOMENT COEFFICIENT WITH AILERON DEFLECTION FOR PARTIALLY SEALED BEVELED AILERON

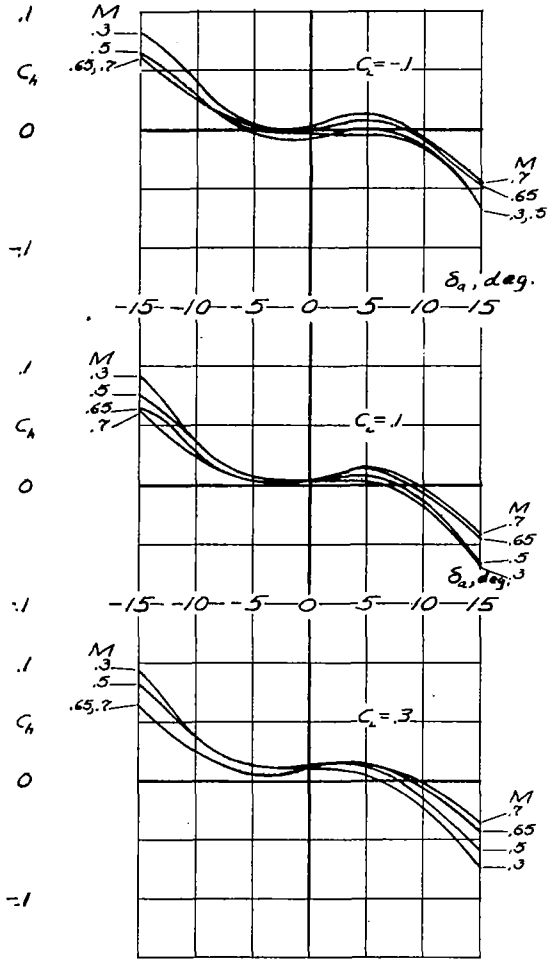

FIGURE 21 - VARIATION OF HINGE-MOMENT COEFFICIENT WITH AILERON DEFLECTION FOR PARTIALLY SEALED BEVELED AILERON

NATIONAL ADVISORY COMMITTEE FOR AERONAUTICS

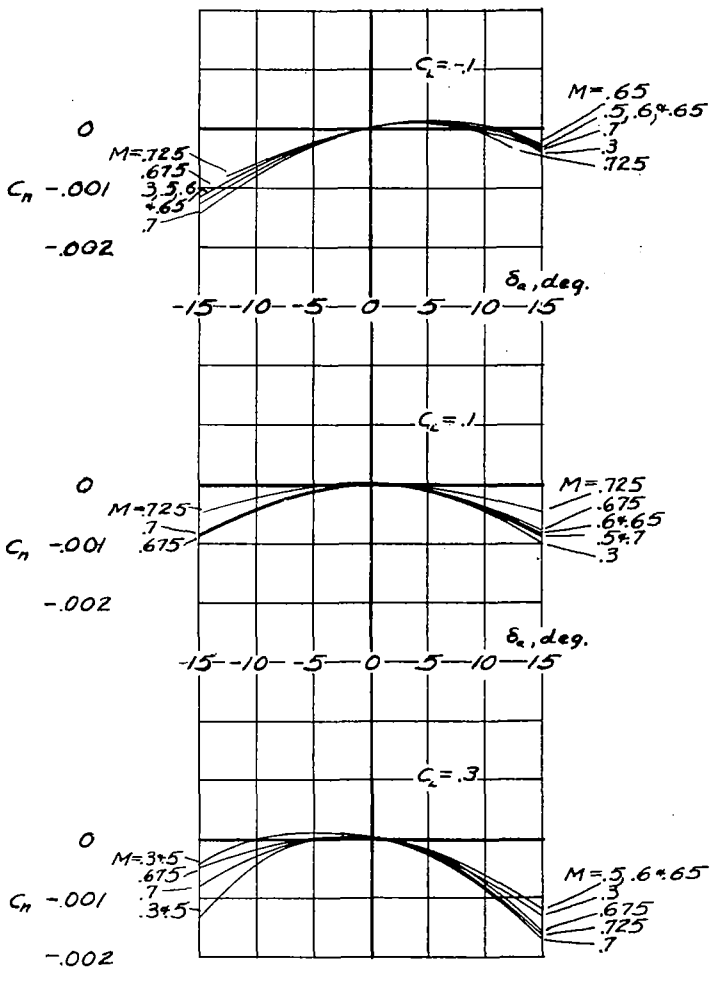

FIGURE 22 - VARIATION OF YAWING-MOMENT COEFFICIENT WITH AILERON DEFLECTION FOR PARTIALLY SEALED BEVELED AILERON

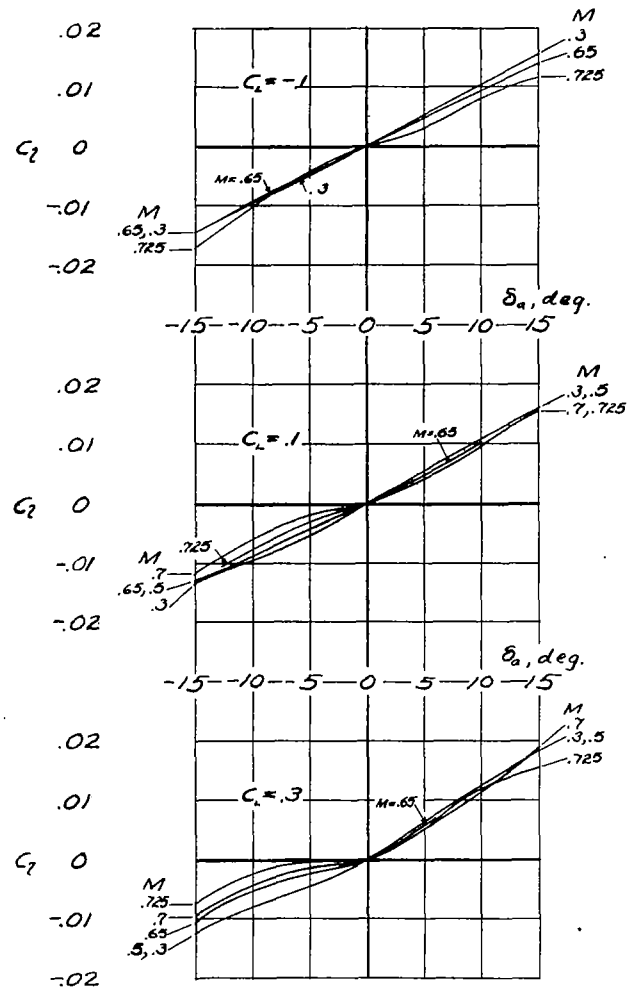

FIGURE 23-VARIATION OF ROLLING-MOMENT COEFFICIENT WITH AILERON DEFLECTION FOR PARTIALLY SEALED BEVELED AILERON. ROUGHNESS AT 0.10 WING CHORD.

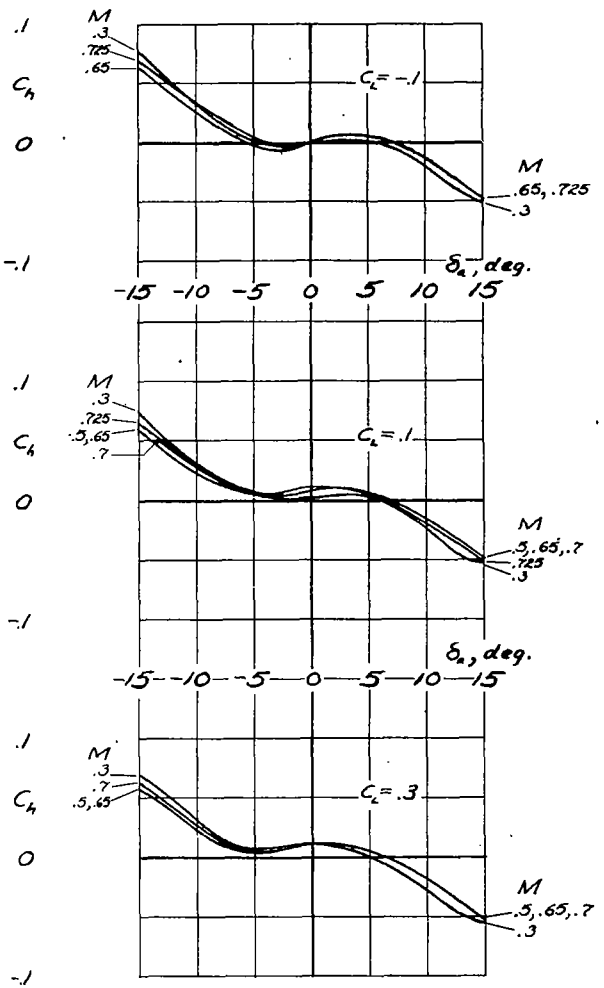

FIGURE 24-VARIATION OF HINGE-MOMENT COEFFICIENT WITH AILERON DEFLECTION FOR PARTIALLY SEALED BEVELED AILERON. ROUGHNESS AT 0.10 WING CHORD.

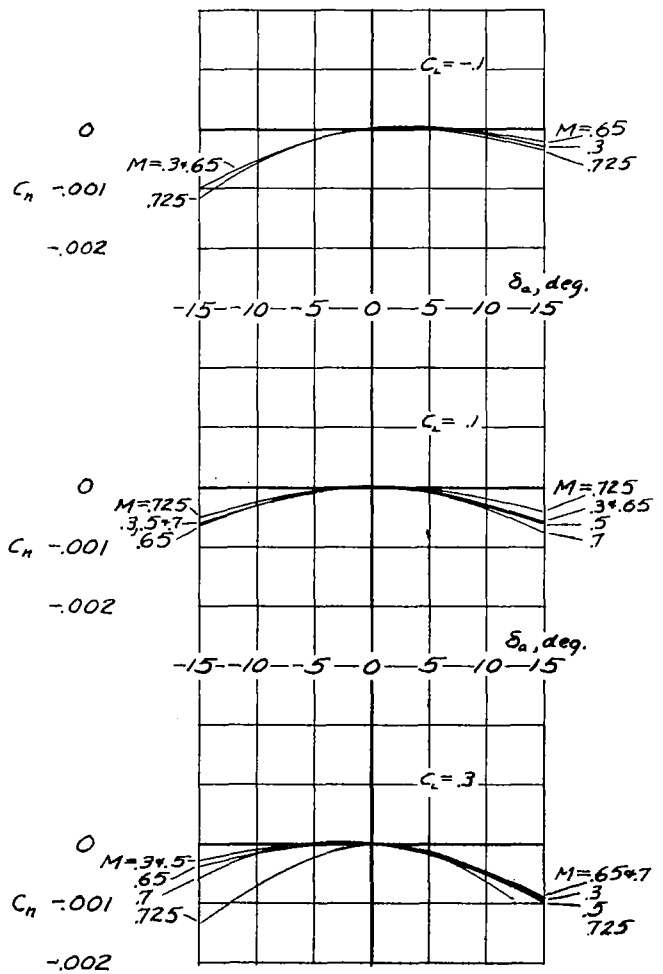

FIGURE 25- VARIATION OF YAWING-MOMENT COEFFICIENT WITH AILERON DEFLECTION FOR PARTIALLY-SEALED BEVELED AILERON. ROUGHNESS AT 0.10 WING CHORD

NATIONAL ADVISORY COMMITTEE FOR AERONAUTICS

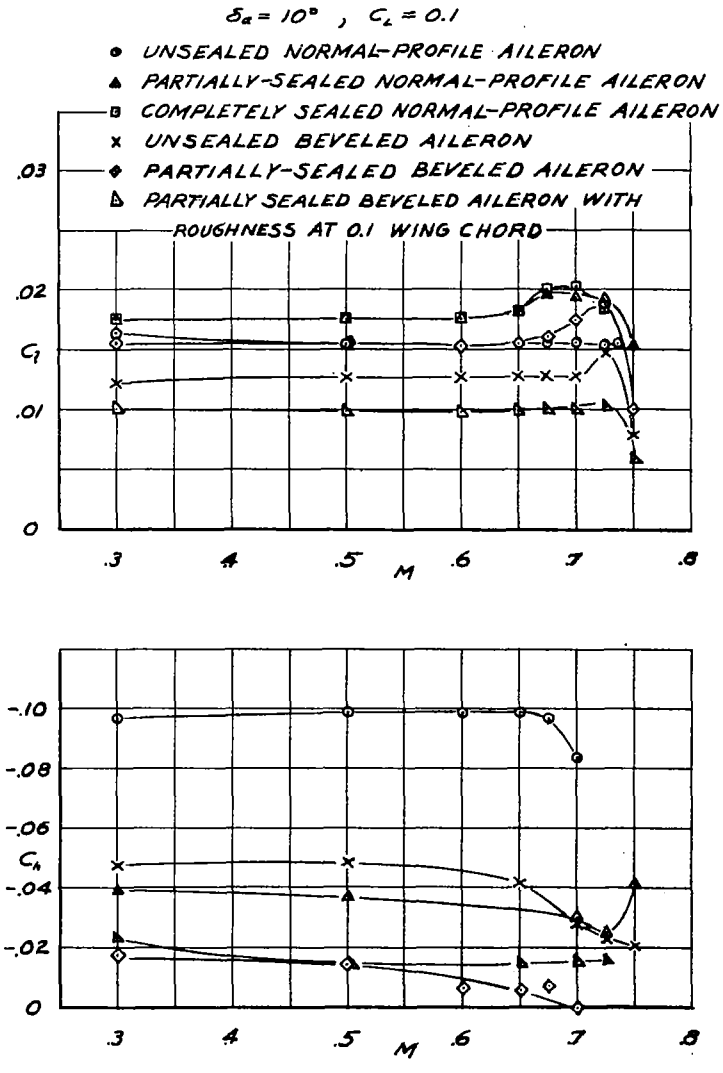

FIGURE 26- EFFECT OF MACH NUMBER ON ROLLING-MOMENT AND HINGE-MOMENT COEFFICIENTS WITH AILERON AT 10°, $C_L = 0.1$

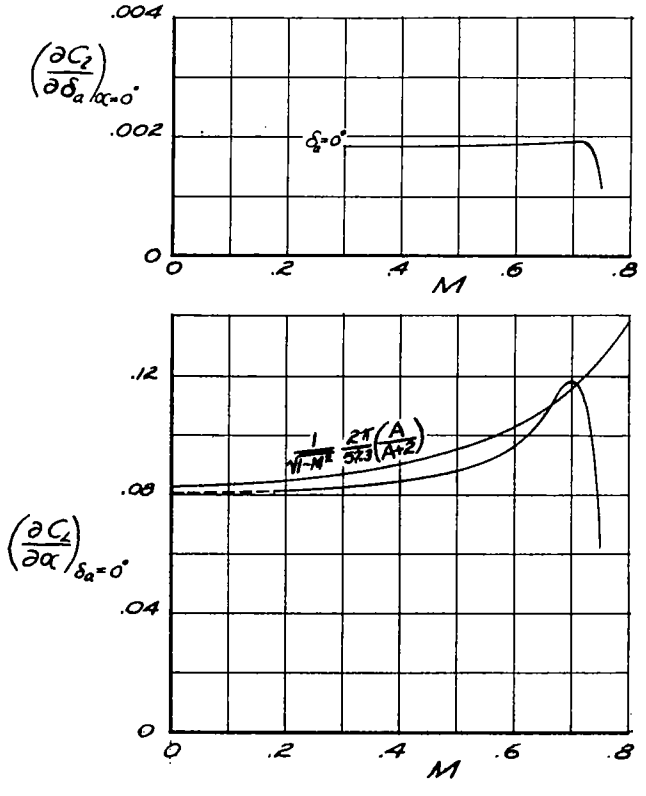

FIGURE 27 - VARIATION OF THE PARAMETERS $\left(\frac{\partial C_l}{\partial \delta_a}\right)_\alpha$ AND $\left(\frac{\partial C_l}{\partial \alpha}\right)_{\delta_a}$ WITH MACH NUMBER FOR THE PARTIALLY SEALED NORMAL-PROFILE AILERON

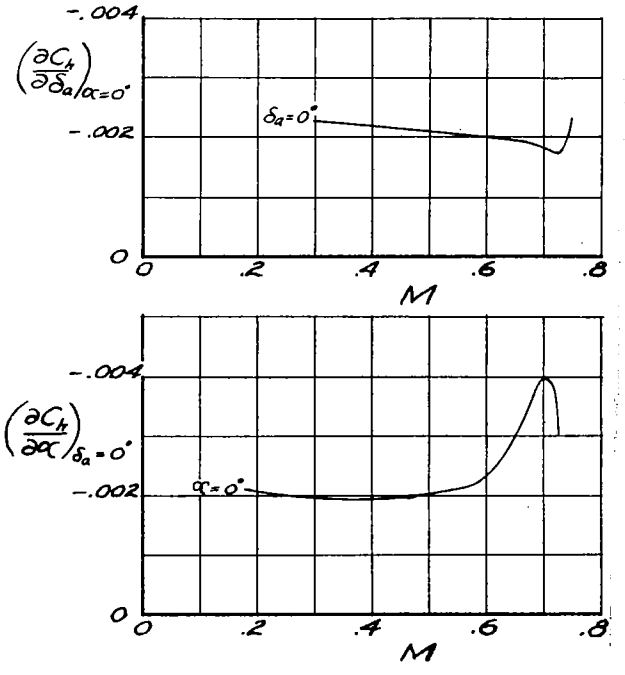

FIGURE 28 - VARIATION OF THE PARAMETERS $\left(\frac{\partial C_h}{\partial \delta_a}\right)_\alpha$ AND $\left(\frac{\partial C_h}{\partial \alpha}\right)_{\delta_a}$ WITH MACH NUMBER FOR THE PARTIALLY SEALED NORMAL-PROFILE AILERON

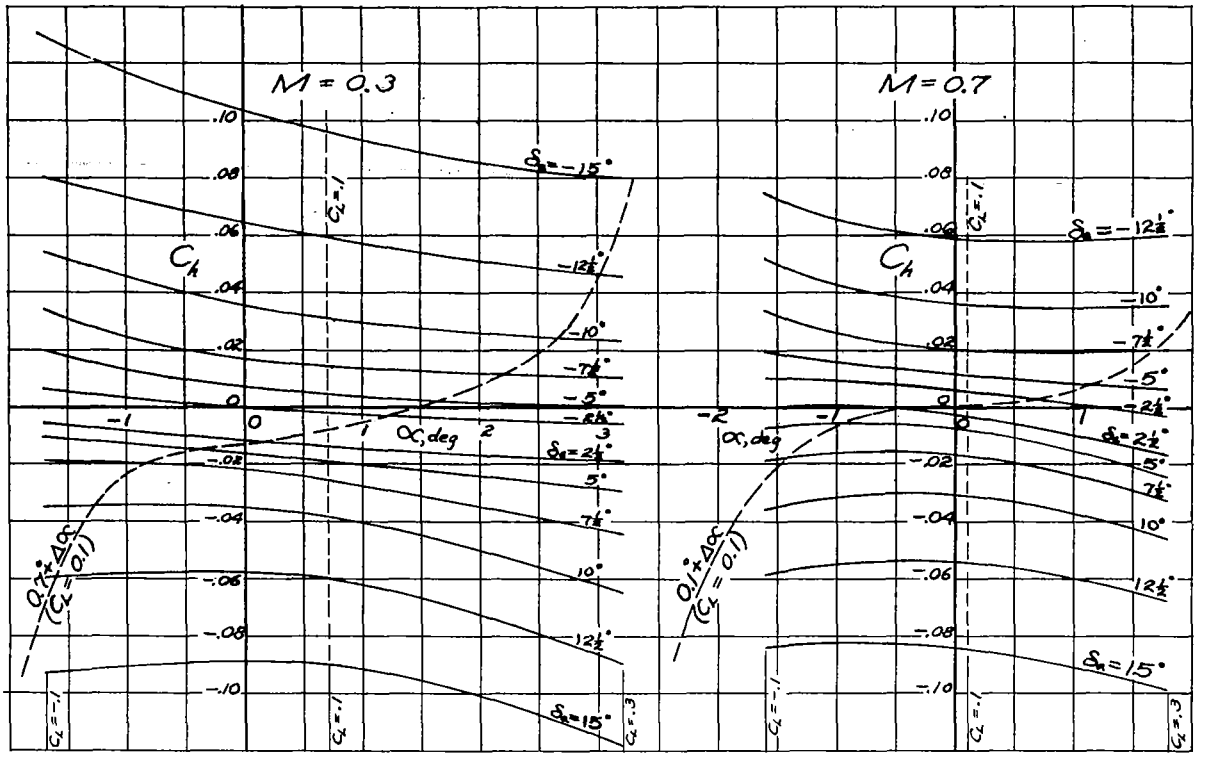

FIGURE 29- VARIATION OF HINGE-MOMENT COEFFICIENT WITH ANGLE OF ATTACK FOR THE PARTIALLY SEALED NORMAL-PROFILE AILERON. TAKEN FROM FIGURE 12 FOR MACH NUMBERS OF .3 AND .7. $\Delta\alpha_{C_L=.1}$ CORRESPONDS TO ROLLING VELOCITY OBTAINED FROM FIG. 11 AND TABLE I.

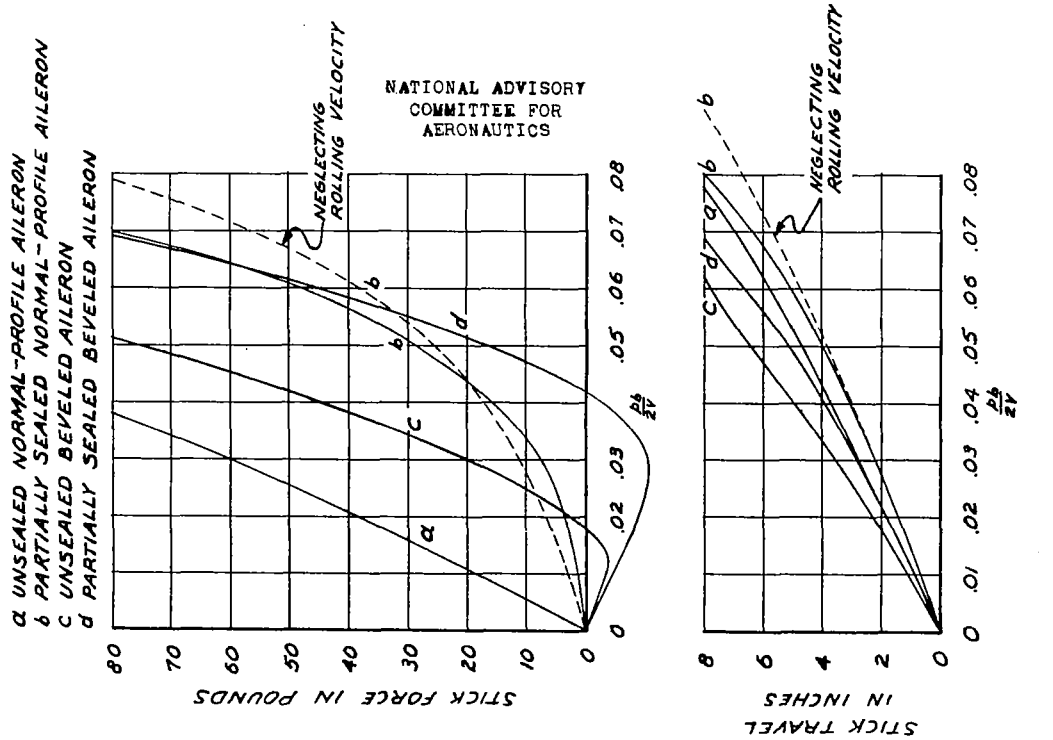

FIGURE 30- AILERON CONTROL CHARACTERISTICS. M = 0.7, C_L = 0.1 q = 337 #/ft², V = 496 mph, V_i = 374 mph, ALTITUDE = 19,900 ft.

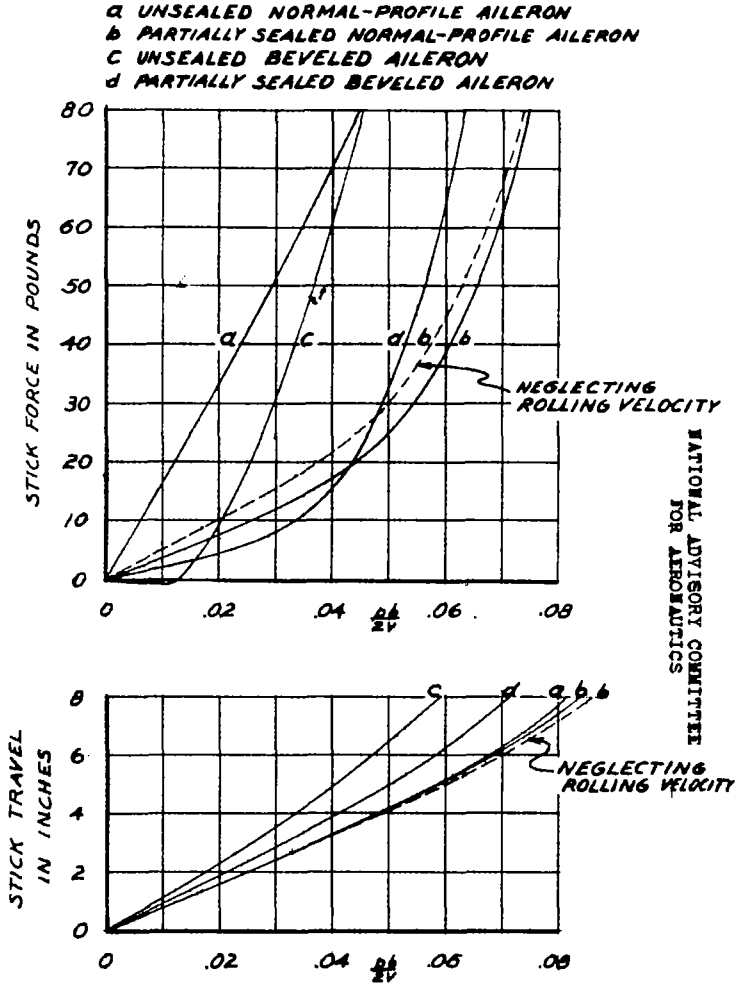

FIGURE 31 - AILERON CONTROL CHARACTERISTICS. $M = 0.3$, $C_L = 0.1$ $q = 337$ #/ft.²

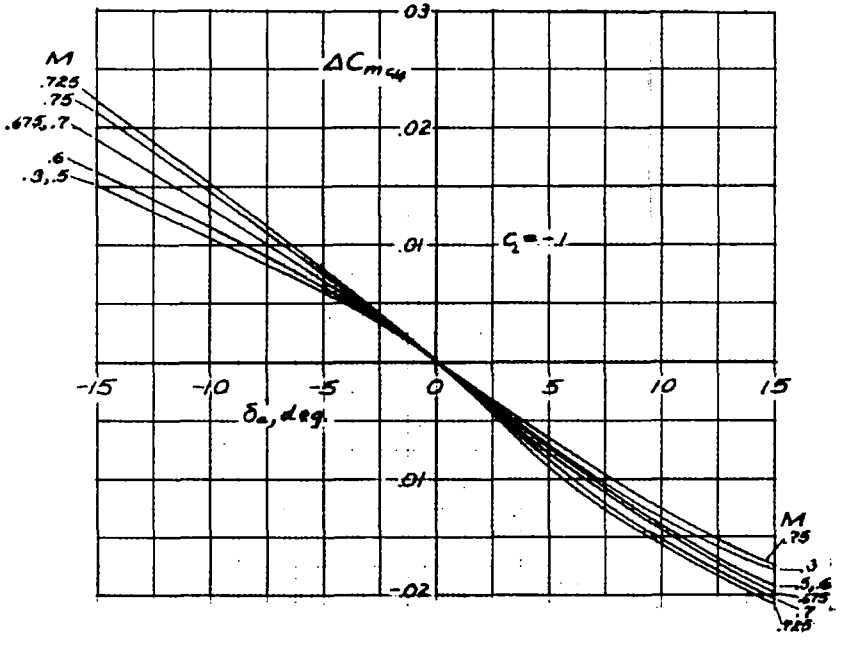

FIGURE 32 - PITCHING-MOMENT COEFFICIENT DUE TO DEFLECTION OF THE PARTIALLY SEALED NORMAL-PROFILE AILERON. $C_L = 0.1$

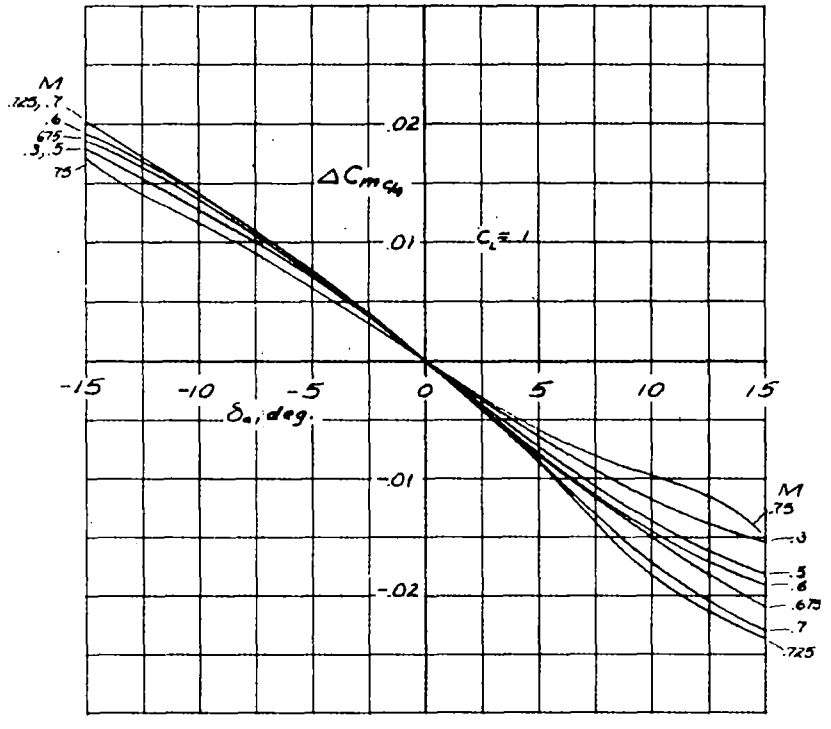

FIGURE 33 - PITCHING-MOMENT COEFFICIENT DUE TO DEFLECTION OF THE PARTIALLY SEALED NORMAL-PROFILE AILERON. $C_L = 0.1$

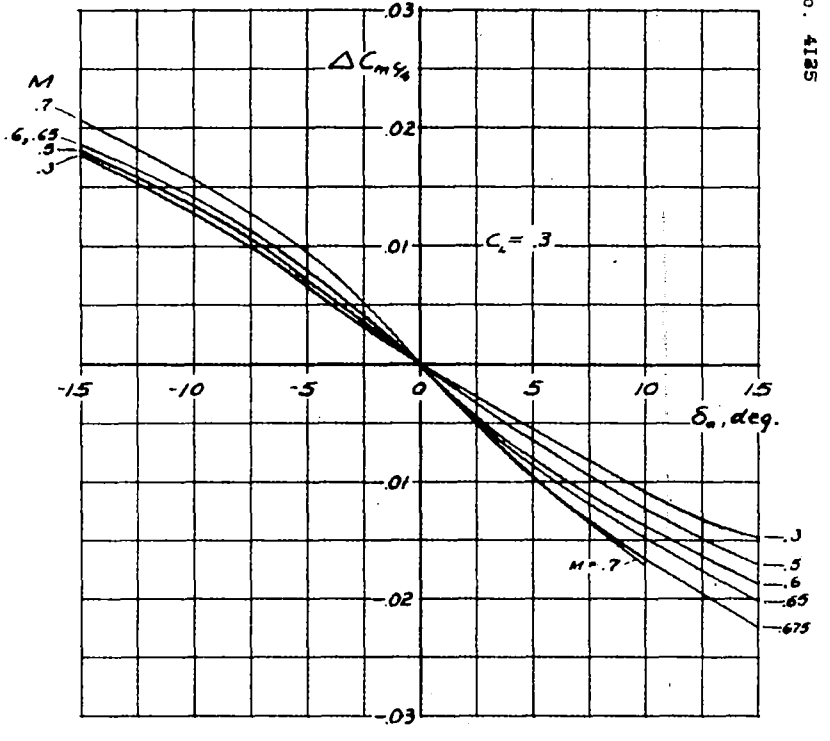

FIGURE 34 - PITCHING-MOMENT COEFFICIENT DUE TO DEFLECTION OF THE PARTIALLY SEALED NORMAL-PROFILE AILERON. $C_L = 0.3$

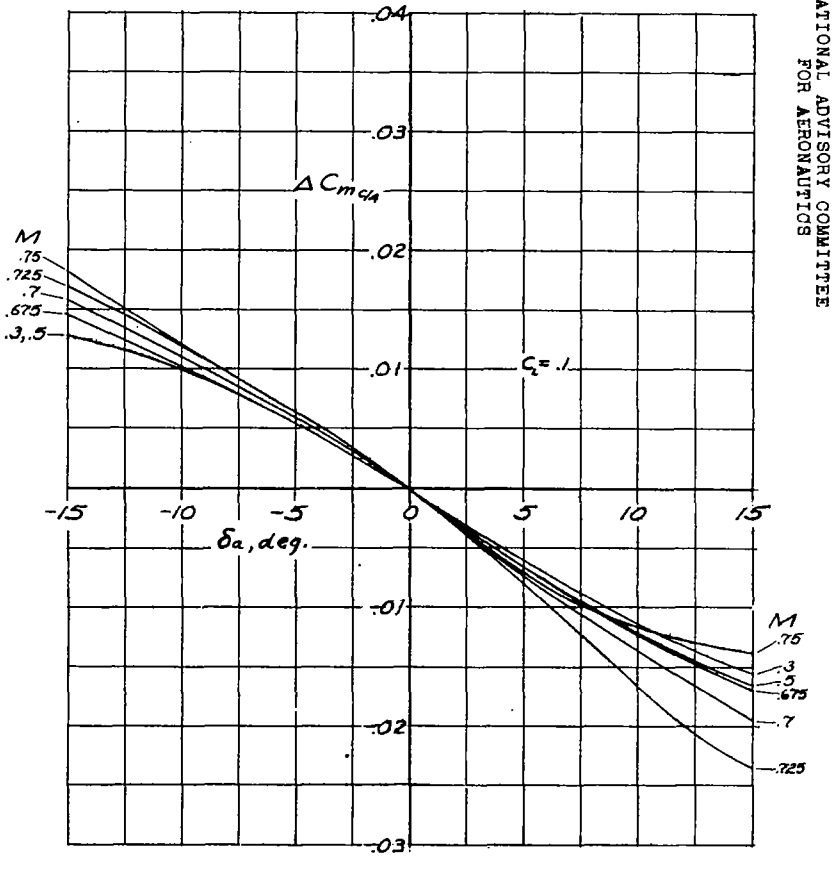

FIGURE 35-PITCHING-MOMENT COEFFICIENT DUE TO DEFLECTION OF THE PARTIALLY SEALED BEVELED AILERON. $C_L = 0.1$

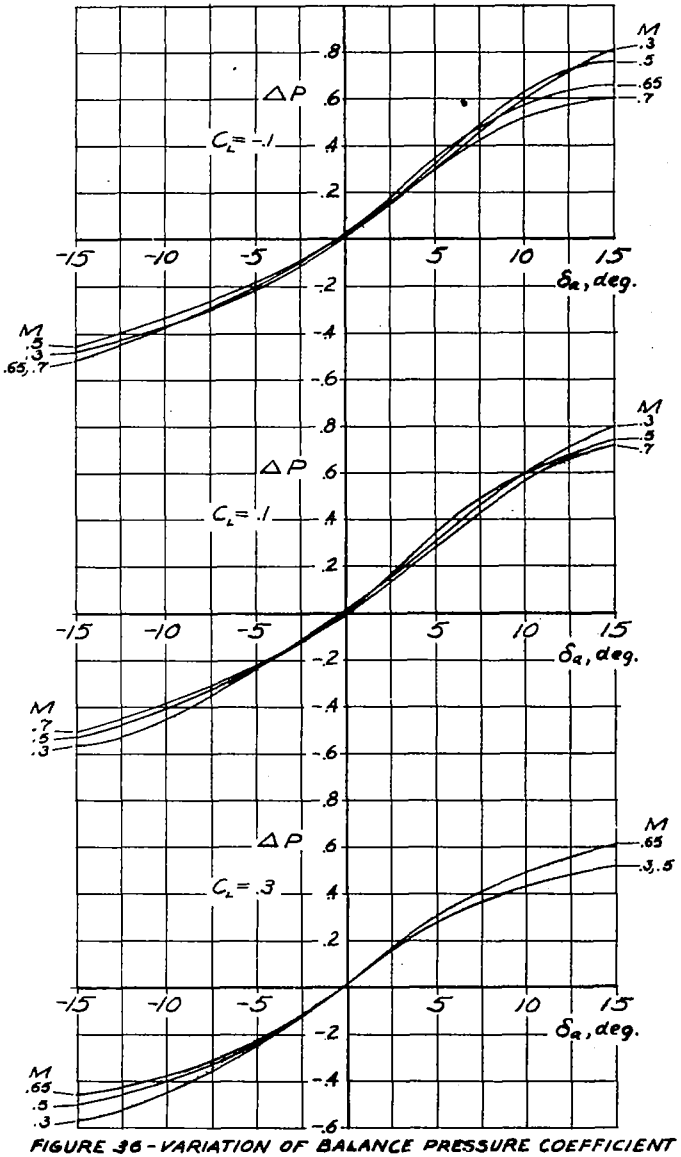

FIGURE 36-VARIATION OF BALANCE PRESSURE COEFFICIENT WITH PARTIALLY SEALED NORMAL-PROFILE AILERON.

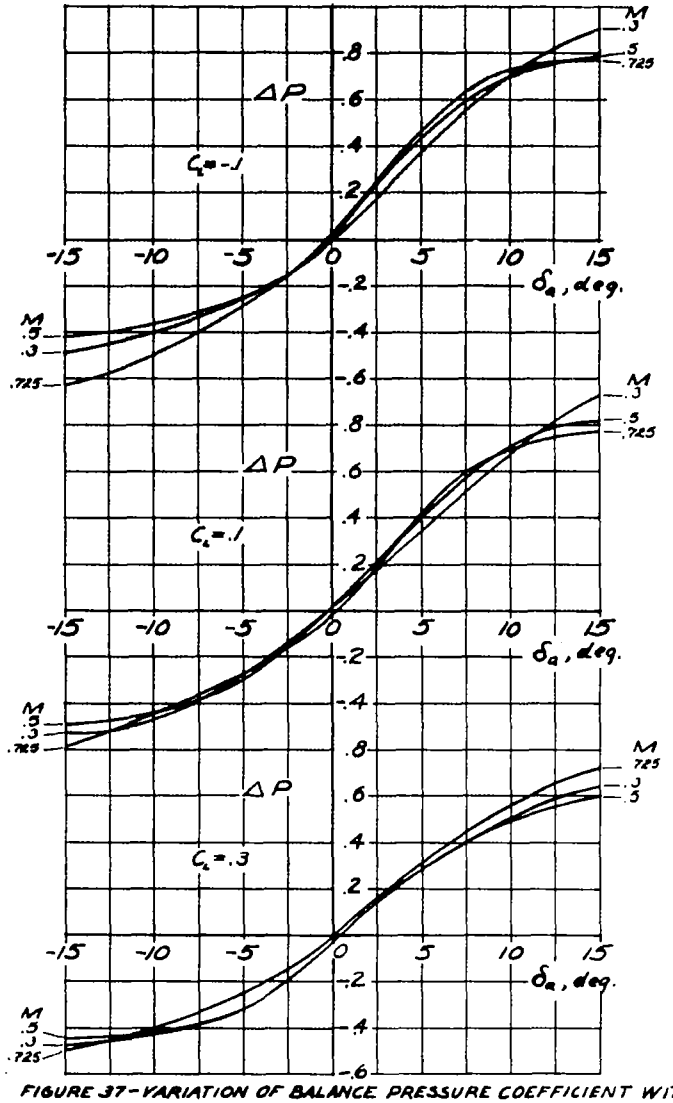

FIGURE 37 - VARIATION OF BALANCE PRESSURE COEFFICIENT WITH DEFLECTION OF PARTIALLY SEALED BEVELED AILERON.

NATIONAL ADVISORY COMMITTEE FOR AERONAUTICS

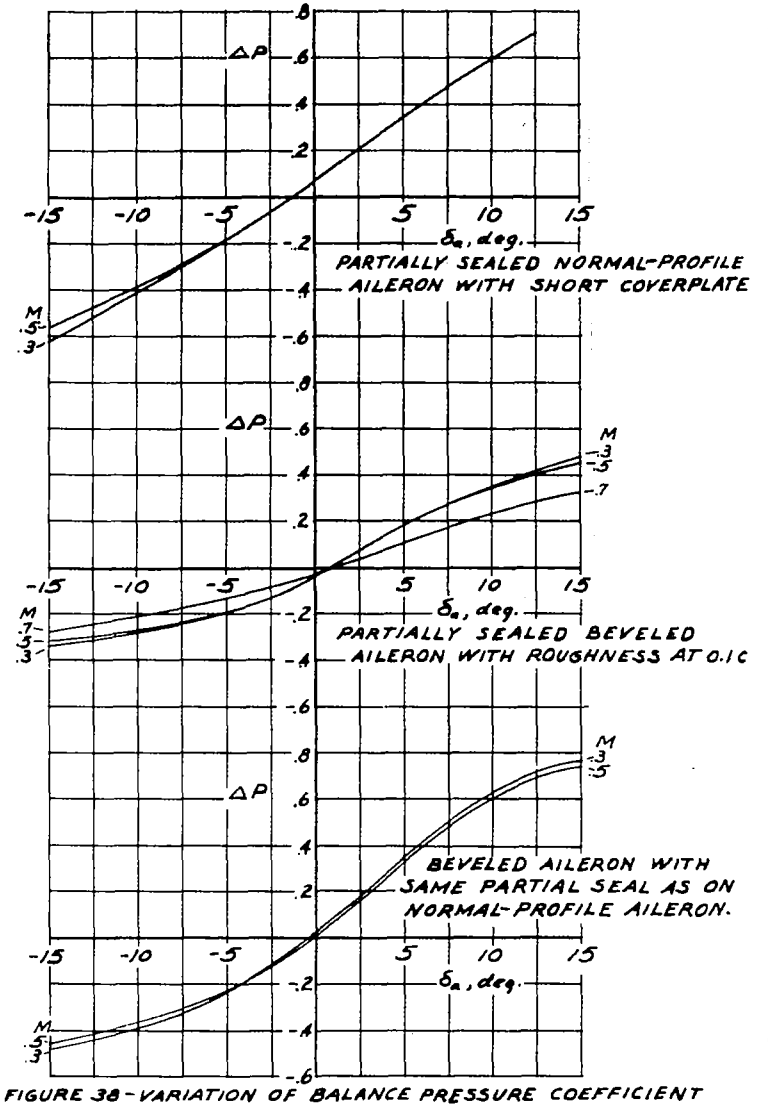

FIGURE 38 - VARIATION OF BALANCE PRESSURE COEFFICIENT WITH AILERON DEFLECTION. C_L = 0.1

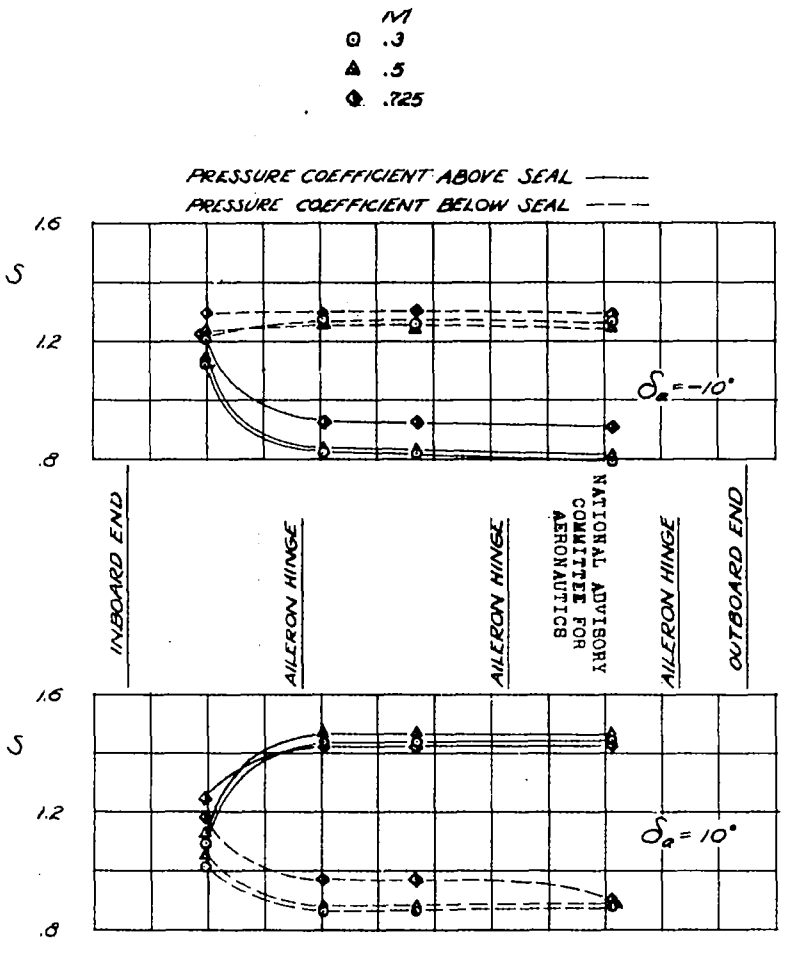

FIGURE 39.- SPANWISE VARIATION OF PRESSURE COEFFICIENT FOR PARTIALLY SEALED NORMAL-PROFILE AILERON. $C_L = 0.1$

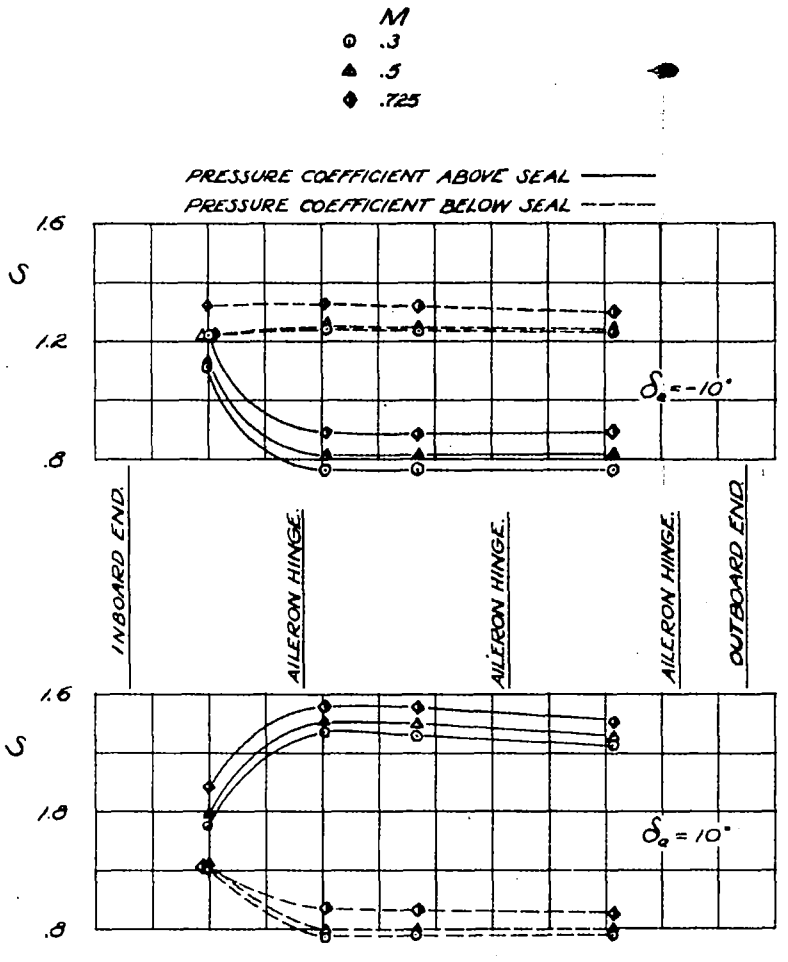

FIGURE 40.- SPANWISE VARIATION OF PRESSURE COEFFICIENT FOR PARTIALLY SEALED BEVELED AILERON. $C_L = 0.1$

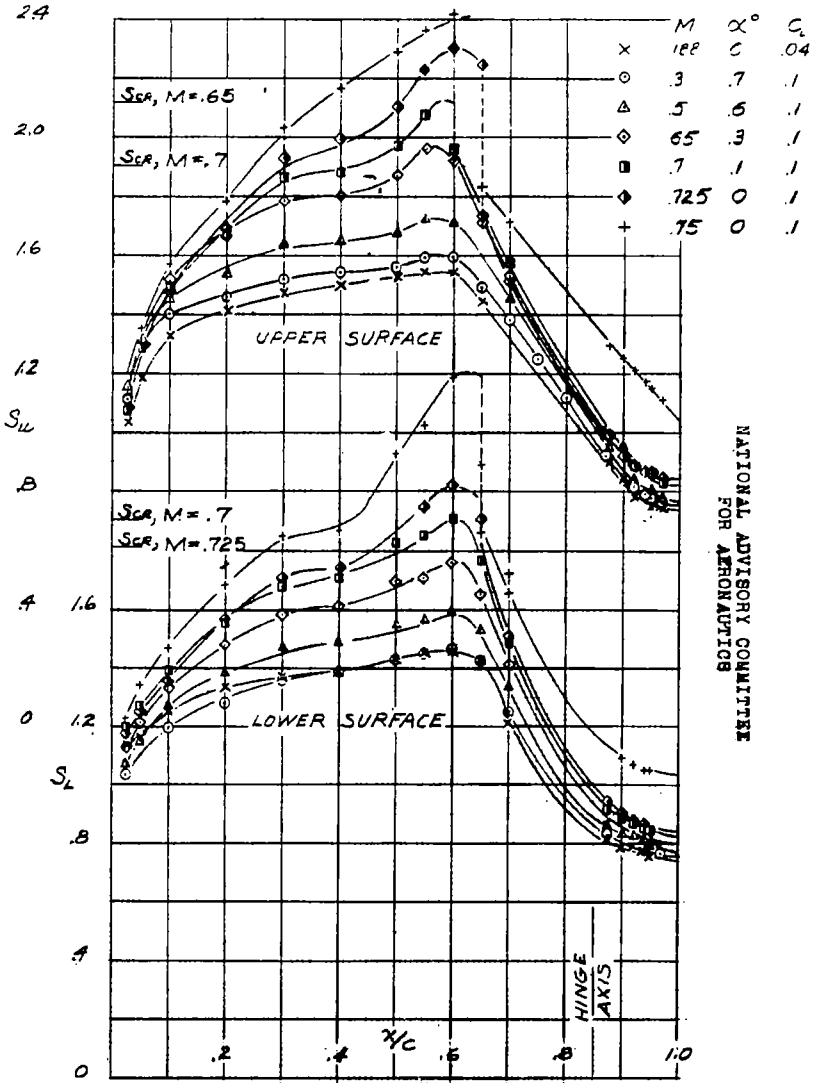

FIGURE 41 - PRESSURE DISTRIBUTION FOR THE PARTIALLY SEALED NORMAL-PROFILE AILERON. $\delta_a = 0°$

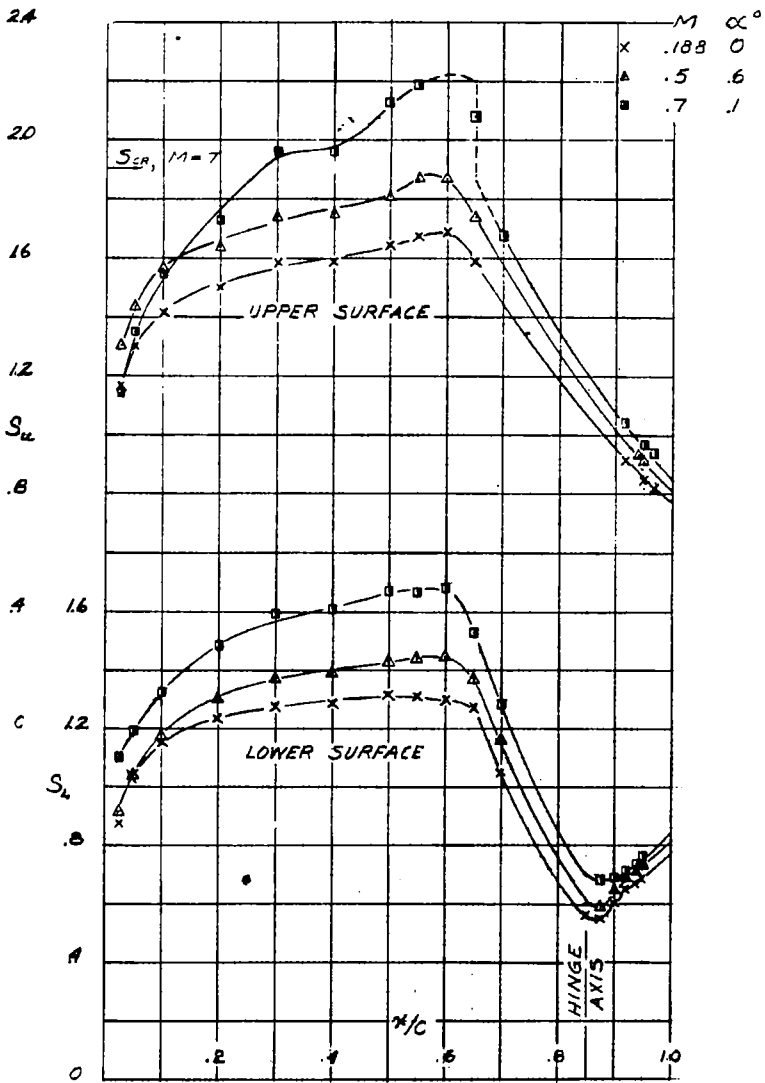

FIGURE 42 - PRESSURE DISTRIBUTION FOR THE PARTIALLY SEALED NORMAL-PROFILE AILERON. $\delta_a = 10°$

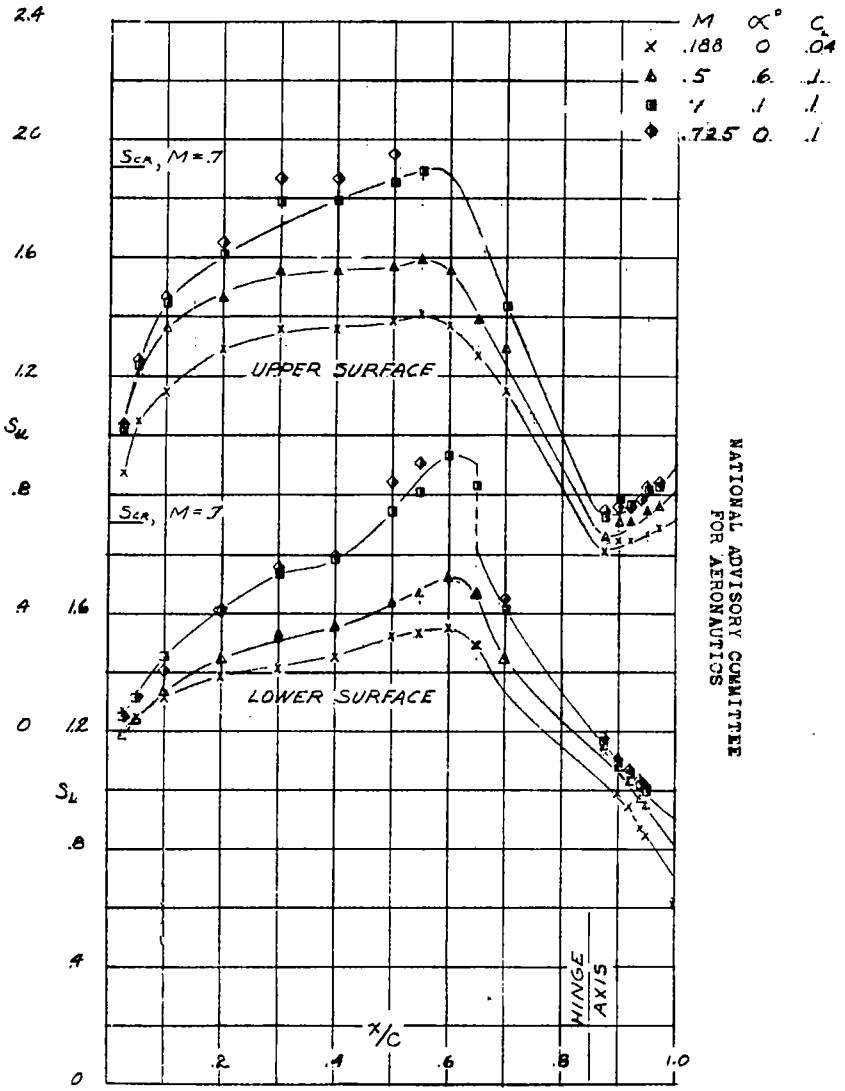

FIGURE 43- PRESSURE DISTRIBUTION FOR THE PARTIALLY SEALED NORMAL-PROFILE AILERON. $\delta_a = -10°$

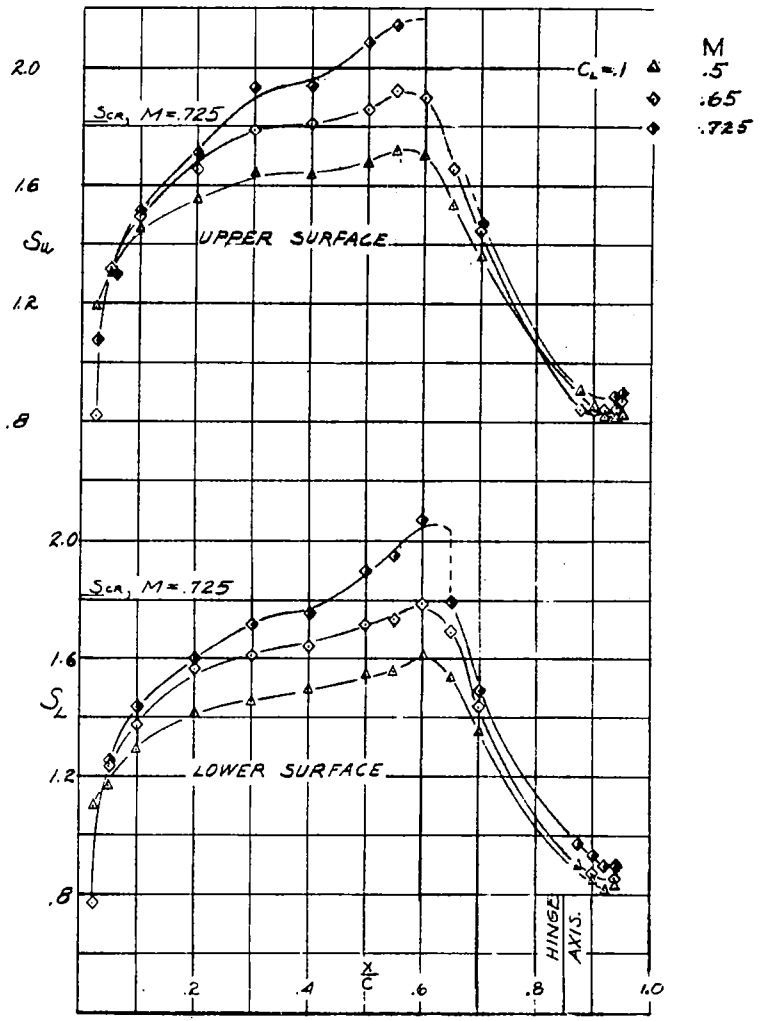

FIGURE 44- PRESSURE DISTRIBUTION FOR THE PARTIALLY SEALED BEVELED AILERON. $\delta_a = 0°$

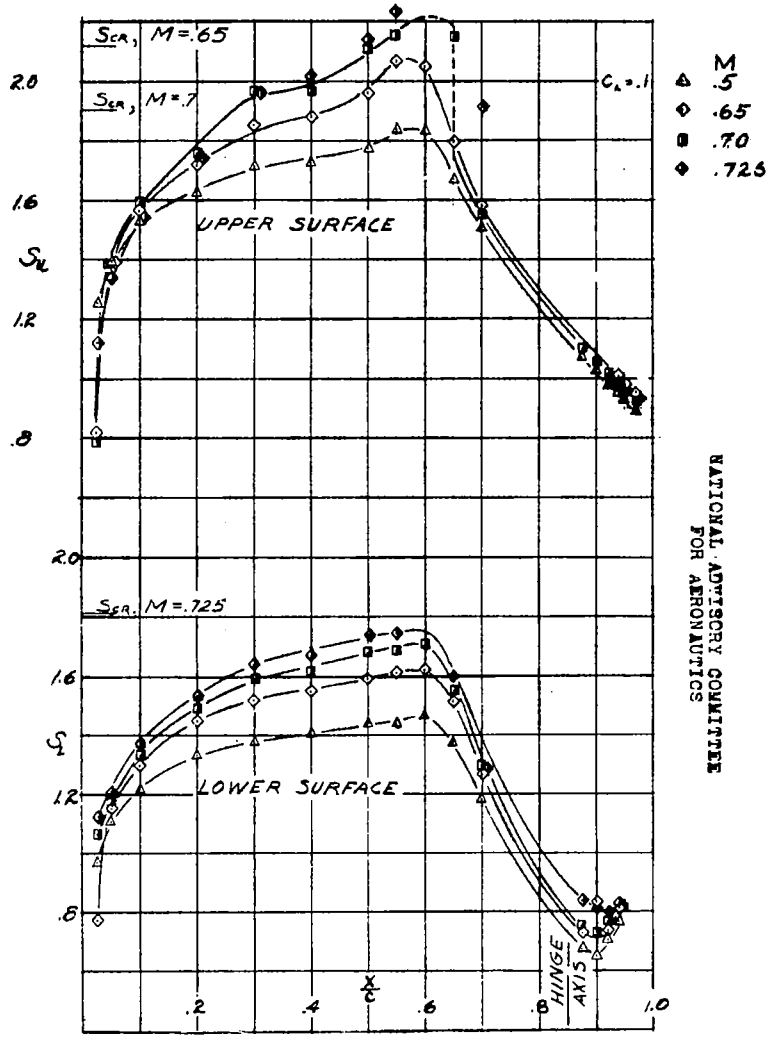

FIGURE 45-PRESSURE DISTRIBUTION FOR THE PARTIALLY SEALED BEVELED AILERON. δ_a= 10°

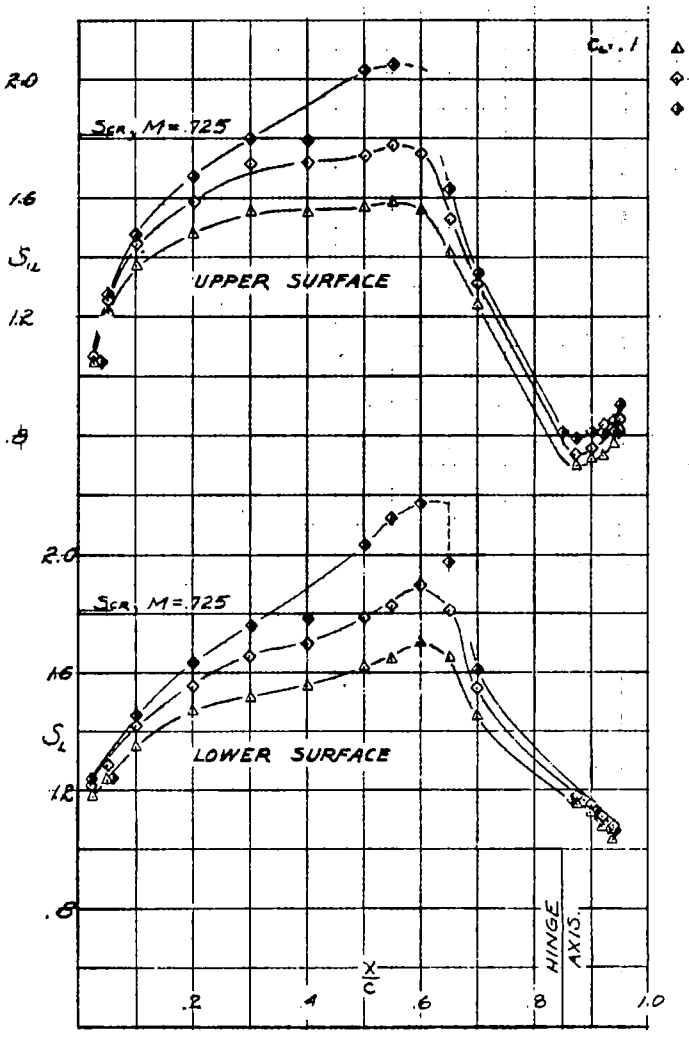

FIGURE 46-PRESSURE DISTRIBUTION FOR THE PARTIALLY SEALED BEVELED AILERON δ_a= -10°

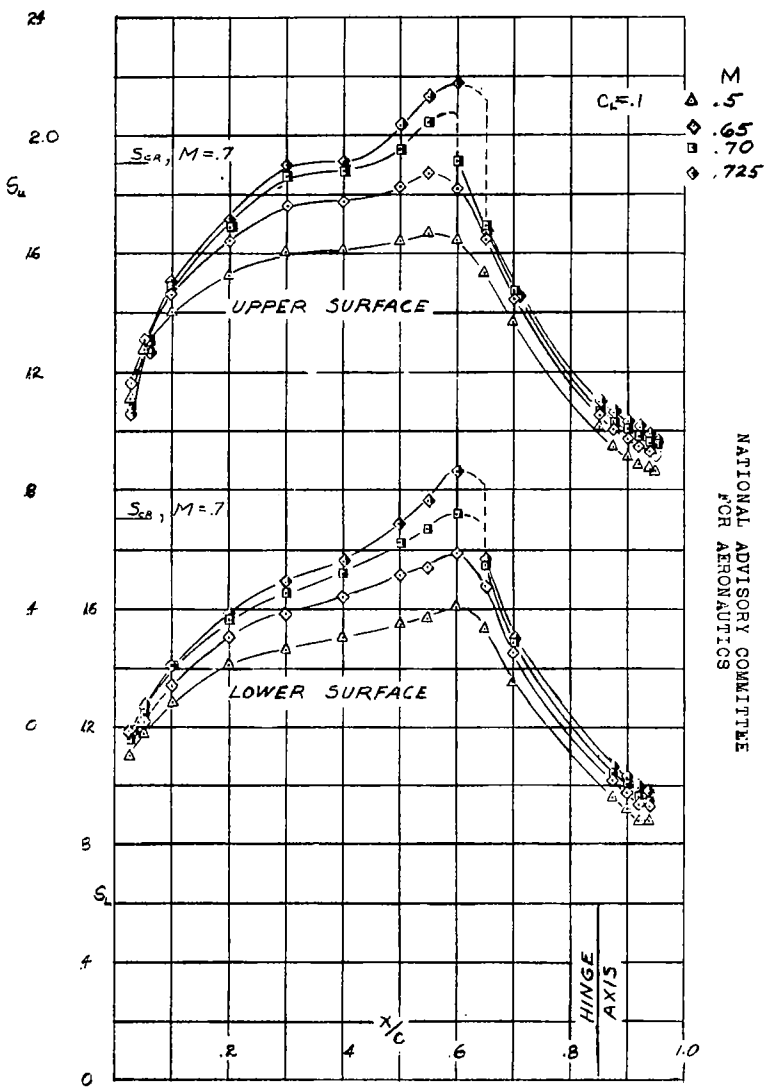

FIGURE 47-PRESSURE DISTRIBUTION FOR THE PARTIALLY SEALED BEVELED AILERON WITH ROUGHNESS AT 0.1 WING CHORD. δ_a=0°

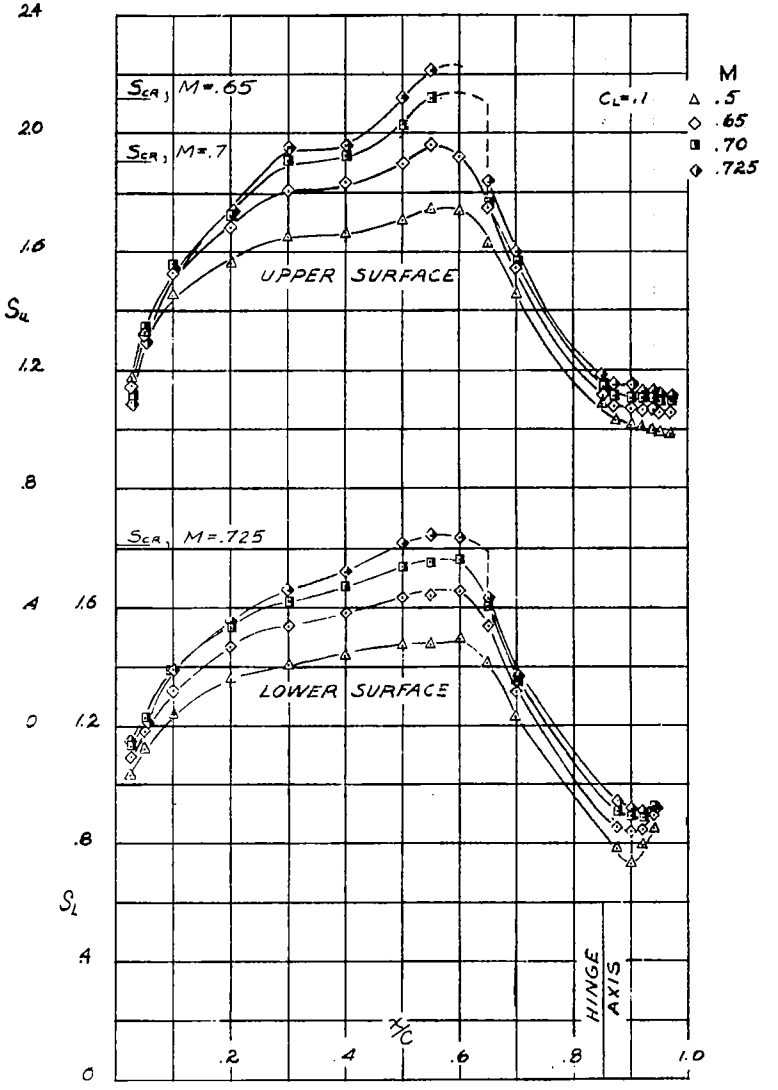

FIGURE 48-PRESSURE DISTRIBUTION FOR THE PARTIALLY SEALED BEVELED AILERON WITH ROUGHNESS AT 0.1 WING CHORD. δ_a=10°

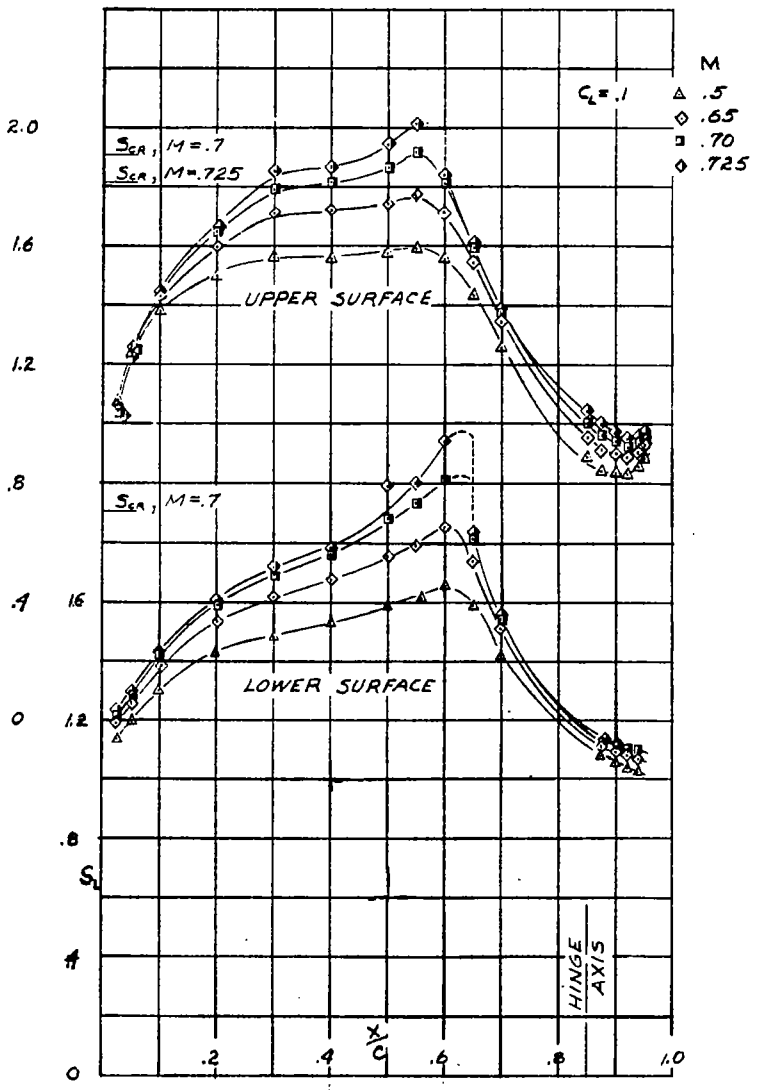

FIGURE 49 - PRESSURE DISTRIBUTION FOR THE PARTIALLY SEALED BEVELED AILERON WITH ROUGHNESS AT 0.1 WING CHORD. $\delta_a = -10°$

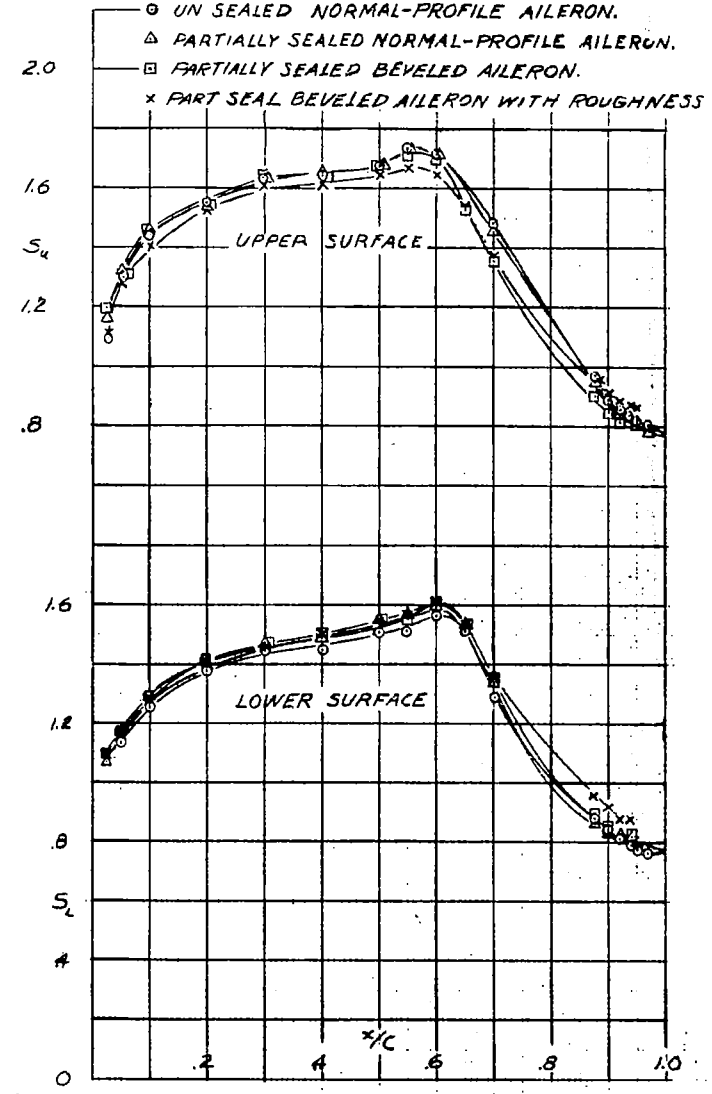

FIGURE 50 - PRESSURE DISTRIBUTION FOR SEVERAL AILERONS $M = 0.5$, $\delta_a = 0°$, $\alpha c = 0.6°$

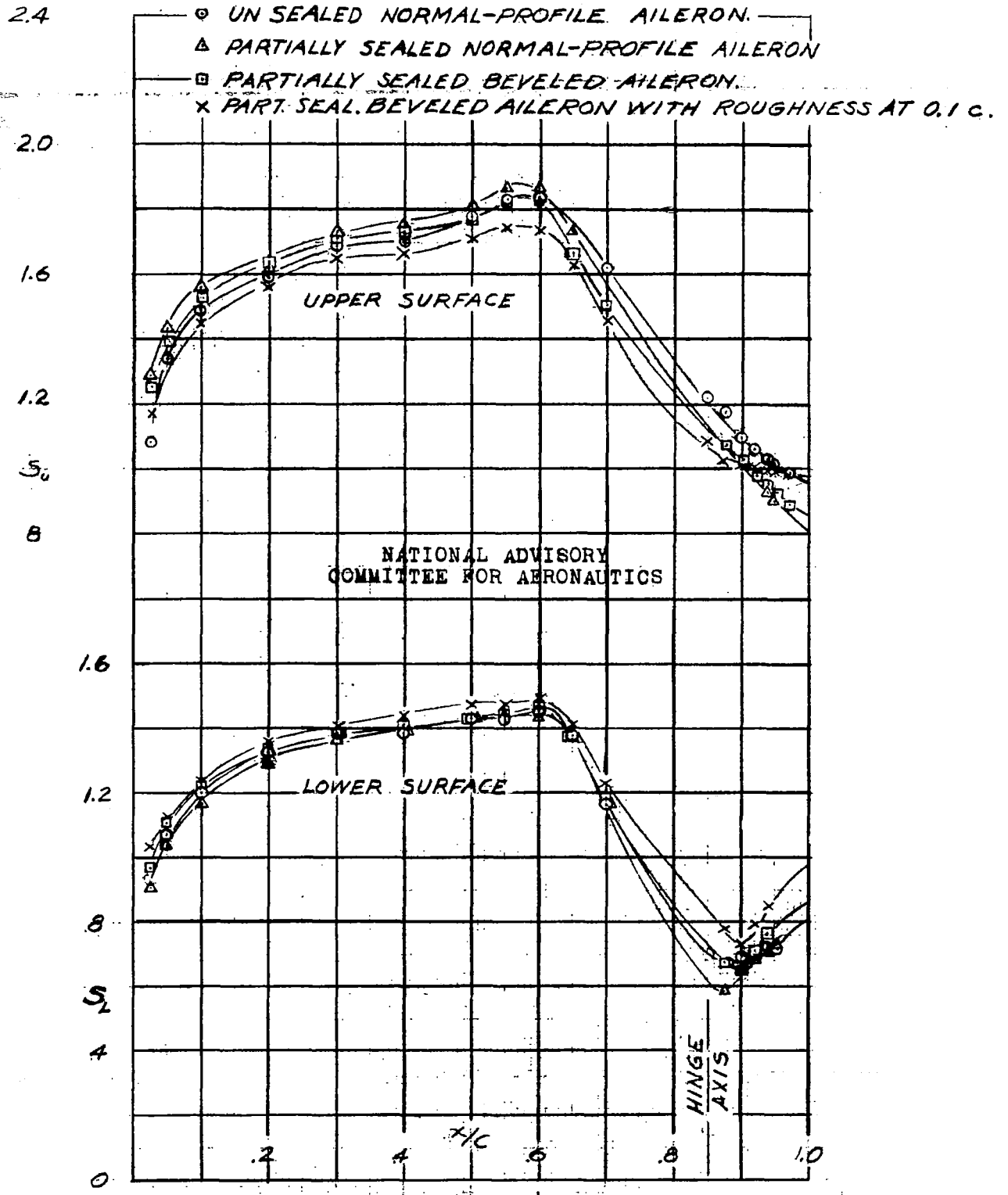

FIGURE 51 - PRESSURE DISTRIBUTION FOR SEVERAL AILERONS
$M = 0.5$, $\delta_a = 10°$, $\alpha = 0.6°$